Energy 44 (2012) 257–277

Contents lists available at SciVerse ScienceDirect

Energy

journal homepage: www.elsevier.com/locate/energy

Fuel quality issues with biogas energy – An economic analysis for a stationary fuel cell system☆

Dionissios D. Papadias*, Shabbir Ahmed, Romesh Kumar

Argonne National Laboratory, Chemical Sciences and Engineering Division, 9700 S. Cass Avenue, Lemont, IL 60439, USA

ARTICLE INFO

Article history:
Received 16 February 2012
Received in revised form
15 May 2012
Accepted 10 June 2012
Available online 12 July 2012

Keywords:
Anaerobic digester gas
Landfill gas
Impurities
Fuel cell system
Impurity removal
Cost analysis

ABSTRACT

This paper reviews the information available on the impurities encountered in stationary fuel cell systems, their effects on the fuel cells, and the maximum allowable concentrations of select impurities suggested by manufacturers and researchers. A generic model of a molten carbonate fuel cell-based power plant operating on digester and landfill gas has been developed; it includes a gas processing unit, followed by a fuel cell system. The model includes the key impurity removal steps to enable predictions of impurity breakthrough, component sizing, and utility needs. These data, along with process efficiency results from the model, were subsequently used to calculate the cost of electricity. Sensitivity analyses were conducted to correlate the concentrations of key impurities in the fuel gas feedstock to the cost of electricity.

1. Introduction

Fuel cell systems are being deployed in stationary applications for the generation of electricity, heat, and hydrogen. These systems use a variety of fuel cell types, ranging from the low temperature PEFC (polymer electrolyte fuel cell) to the high temperature SOFC (solid oxide fuel cell). Depending on the application and location, these systems are being designed to operate on reformate or syngas produced from various fuels that include natural gas, biogas, coal gas, etc. All of these fuels contain species that can potentially damage the fuel cell anode or other unit operations and processes that precede the fuel cell stack. These detrimental effects include loss in performance or durability, and attenuating these effects requires additional components to reduce the impurity concentrations to tolerable levels, if not eliminate the impurity entirely. These impurity management components increase the complexity of the fuel cell system, and they add to the system's capital and operating costs (such as regeneration, replacement and disposal of spent material and maintenance).

This work reviewed the public domain information available on the impurities encountered in stationary fuel cell systems, and the effects of the impurities on the fuel cells. A database has been set up that classifies the impurities in renewable fuels, such as landfill gas and anaerobic digester gas from wastewater treatment plants. The work documents the known deleterious effects on fuel cells, and the maximum allowable concentrations of select impurities suggested by manufacturers and researchers. The literature review helped to identify the impurity removal strategies that are available, and their effectiveness, capacity, and cost. A generic model of a molten carbonate fuel cell-based power plant operating on digester and landfill gas has been developed; it includes a gas processing unit, followed by a fuel cell system. The model includes the key impurity removal steps to enable predictions of impurity breakthrough, component sizing, and utility needs. These data, along with process efficiency results from the model, were subsequently used to calculate the cost of electricity. Sensitivity analyses were conducted to correlate the concentrations of key impurities in the fuel gas feedstock to the cost of electricity.

2. Biogas resources

Waste-derived fuels are attracting attention as a renewable source of energy, and they are being considered as feedstock for stationary power and CHP (Combined Heat and Power) systems.

☆ The U.S. Government retains for itself, and others acting on its behalf, a paid-up, nonexclusive, irrevocable worldwide license in said article to reproduce, prepare derivative works, distribute copies to the public and perform publicly and display publicly, by or on behalf of the Government.

* Corresponding author. Tel.: +1 630 252 3206.
E-mail address: papadias@anl.gov (D.D. Papadias).

0360-5442/$ – see front matter © 2012 Published by Elsevier Ltd.
http://dx.doi.org/10.1016/j.energy.2012.06.031

Acronyms

AC	activated Carbon
ADG	anaerobic digester gas
DMS	dimethyl sulfide
Dx	cyclic organosilicon compound
GPU	gas processing unit
IAST	ideal adsorbed solution theory
Lx	linear organosilicon compound
LFG	landfill gas
LHV	lower heating value of fuel
MCFC	molten carbonate fuel cell
MGD	million gallons per day
MSW	municipal solid waste
OAC	ordinary activated carbon
PAFC	phosphoric acid fuel cell
PEFC	polymer electrolyte fuel cell
SCF	standard cubic foot
SOFC	solid oxide fuel cell
SMR	steam methane reforming
VOC	volatile organic compound
WGS	water gas shift
WWTP	wastewater treatment plant

Notation

C	gas phase concentration of reactant (mol m^{-3})
C_B	molar density of solid based on maximum adsorption capacity (mol m^{-3})
d_p	particle diameter (m)
D_e	diffusivity in reacted layer (m^2 s^{-1})
D_L	axial dispersion coefficient (m^2 s^{-1})
k_f	gas-to-solid mass-transfer rate (m s^{-1})
k_v	Volume adjusting coefficient (−)
L	reactor length (m)
P	partial pressure of adsorbate in the gas phase (atm)
P_v	vapor pressure of adsorbate (atm)
q	adsorption capacity per mass activated carbon (mol g^{-1})
R_0	radius of adsorbent particle, m^{-1}
R	radius of inner unreacted core of the adsorbent particle (m)
T	temperature (K)
U_0	superficial velocity in bed (m s^{-1})
V_b	molar volume of the adsorpbate at its normal boiling point (cm^3 mol^{-1})
V_0	active adsorption space, micropore volume of carbon (cm^3 g^{-1})

Greek symbols

β	affinity coefficient (−)
ε_b	bed porosity (−)
σ	external surface area of particle per unit volume in the bed (m^2 m^{-3}) $\sigma = 6(1-\varepsilon_B)/d_p$

General waste streams considered in this paper include ADG (anaerobic digester gas) from wastewater treatment plants and LFG (landfill gas) from municipal solid waste.

Landfill gas has been the subject of numerous studies around the world and the U.S. EPA (Environmental Protection Agency) has published a large amount of data that it has collected over the years [1]. Landfill gas is the by-product of the decomposition of organic matter (e.g., paper, food scraps, plastics and yard trimmings) in MSW (municipal solid waste). The total MSW generated in the U.S. in 2009 was 243 million tons, of which, approximately 54% was deposited in landfills [2]. Besides MSW, other wastes may also be landfilled, including construction and demolition debris, wastewater sludge, and non-hazardous industrial waste.

When waste is deposited in a landfill, it undergoes a series of decomposition phases during a period of approximately 1 year [3]. Initially, aerobic decomposition takes place where oxygen is consumed forming carbon dioxide, water and heat. Upon oxygen depletion, anaerobic decomposition takes place where the final phase is characterized by a steady production of LFG. This gas is typically saturated with water vapor, and it contains mainly methane (40–60%) and carbon dioxide (35–50%), with smaller amounts of oxygen (<1%) and nitrogen (3–5%) [4,5]. One million tons of MSW produce approximately 430,000 scf (standard cubic feet) per day of LFG for 20–30 years after being deposited in the landfill. Of the nearly 2300 landfills in the U.S., there are currently ~550 operational projects in 40 states that collect landfill gas to produce 1727 MW of electric power (most of which is generated with internal combustion engines) and 312 million scf/day of fuel gas for commercial and residential heating. There are another ~500 candidate sites that could produce an additional 1170 MW of electricity [6].

Anaerobic digestion is commonly employed in many WWTP (wastewater treatment plants) to biochemically stabilize the sludge before final treatment and disposal [7,8]. Anaerobic microorganisms first hydrolyze the solids/sludge followed by a fermentation process to yield simpler organic acids. In subsequent steps of AD (anaerobic digestion), acids are further digested to form acetic acid as well as H_2 and CO_2. The last stage of the digestion process is characterized by the production of methane. Here a group of methanogenic bacteria splits acetic acid to methane and CO_2 and the other group of bacteria uses hydrogen and CO_2 to form methane. The production rate of biogas from mixed sludge is typical in the range of 0.75–1.12 m^3 per kg VS (volatile suspended solids) destroyed (12–18 cf/lb VS destroyed) [7,9]. The biogas has an average methane content of ~60%, with the balance of the biogas consisting primarily of CO_2 [7,8].

Digesters are most often operated in two temperature ranges, (a) mesophilic range (30–37 °C) and (b) thermophilic range (50–60 °C) which primarily affect the decomposition rate and heat addition to the process [7,9,10]. Mesophilic digesters are most commonly applied for anaerobic sludge digestion in North America [9]. These digesters are operated at organic loading rates in the range of 1.6–3.2 kg-VS/m^3, day (0.013–0.027 lb/gal, day). The degradation of VS (volatile suspended solids) in mesophilic anaerobic process is about 40–50% at retention times between 15 and 25 days. Compared to mesophilic digestion, thermophilic digesters have the advantage of shorter retention times (10–12 days), higher loading rates (3–8.7 kg-VS/m^3, day) as well as higher VS reduction. The disadvantages compared to mesophilic digesters include higher heating cost, higher odor content and higher susceptibility to process variations.

Typically, approximately 1 scf of biogas is produced per 100 gallons of wastewater treated [10]. The EPA Combined Heat and Power Partnership estimates that energy recovery is not economically feasible for treatment plants with capacities of less than 5 MGD (million gallons per day) [10]. Of the nearly 16,000 publically owned treatment facilities in the U.S., about 1000 treat >5 MGD, as shown in Table 1 [10]. While anaerobic digestion is used for ~60%

Table 1
Capacity and ADG utilization of wastewater treatment plants in the U.S. Influx classified by flow rate [10].

WWTPs by flow rates (MGD)	Total WWTPs	Total wastewater flow (MGD)	Wastewater flow to WWTPs with ADG (MGD)	WWTPs with ADG utilizing biogas (%)	Power wasted[a] (MWth)
>200	15	5147	3783	50	159
100–200	26	3885	2652	53	84
75–100	27	2321	1350	44	52
50–75	30	1847	1125	28	56
20–50	178	5375	2573	29	132
10–20	286	3883	2039	13	125
5–10	504	3489	1728	15	103
Total	**1066**	**25,945**	**15,247**	**19**	**711**

[a] Power not utilized for WWTPs with ADG. Power calculated assumes 60% methane in biogas, and 1 ft^3-biogas generated for every 100 gallon water treated (70 kWth/MGD).

of the total combined flow for all plants, a significant part of the gas is not utilized. This is especially so for plants with capacities below 75 MGD.

Utilizing the energy content of the ADG may offset a large part of the WWTPs' power requirements. Fig. 1 shows the electrical power consumption for activated sludge treatment plants including a breakdown of the main power requirements, where pumps and blowers account for the bulk of the energy needs [8]. For instance, a 10 MGD plant that consumes 468 kWe and produces a biogas with an energy content of 700 kWth (LHV (lower heating value of fuel)[1]) would need to convert the fuel at ~0.67 efficiency to offset all electrical power demand. By using fuel cells to convert the biogas to electricity,[2] in combination with other plant energy improvements, such as improving pumping efficiency [11], it is possible to recover a substantial fraction, if not most of the energy need of the WWTPs.

3. Impurities

The higher temperature fuel cells are capable of internal reforming, where some of the lighter hydrocarbons are converted to hydrogen and carbon oxides within the anode chamber [12]. These latter types of fuel cell systems require pre-processing of the fuel to breakdown the complex hydrocarbons into a reformate containing light hydrocarbons, hydrogen, and carbon oxides. The conversion of the feedstock to a fuel gas (reformate) suitable for the type of fuel cell is accomplished by an appropriate fuel processor, and includes unit operations and processes to increase the concentration of hydrogen and reduce that of the impurities. This study will define impurities as any chemical species that does not participate in the electrochemical oxidation reaction to generate electric power. Thus, CO may not be considered an impurity in the high temperature fuel cells such as solid oxide and carbonate fuel cells.

Waste-derived fuels contain a variety of trace contaminants, some of which are produced by biological digestion, while others are volatilized from the waste stream being digested. The contaminant matrix can be complex, containing several hundred species that can damage the fuel cell anode (Table 2 lists impurity tolerance limits for high temperature fuel cells for some of the impurities of concern) or other unit operations and processes that precede the fuel cell stack. The amount and speciation of such trace contaminants depends on various factors, such as the type and age of waste, temperature and pressure, and the stage of the decomposition process [4,13–15].

We have reviewed the published data on low level impurities present in LFG and ADG and have set up a database [16] that includes nearly 300 impurity species found in the biogas matrix. The database classifies the impurities (such as sulfur, siloxanes, halogens, and aromatics) and provides links to specific properties of the species. The database breaks down the information by location, the number of data points on each species, and the minimum, maximum, and average concentrations of the species, as well as information regarding the refuse type, flow rates, and origin and age of waste. Although a direct comparison between the biogas sources would be impractical – as each waste source shows great variability in trace components – it is possible to identify the similarities and differences on an average basis among the various biogas sources.

While many contaminant species are present in biogas, three classes of impurities were found to be of particular concern when used in fuel cells (or combined heat and power) systems: sulfur, siloxanes, and VOCs (volatile organic compounds).

3.1. Sulfur

Reduced sulfur compounds are common and often present in significant concentrations in all biogas sources. Most often, sulfur is present as H_2S (hydrogen sulfide) at concentrations up to several thousand parts per million by volume. The highest level of sulfur is found in ADG of dairy streams, where it can range from 500 to 3000 ppm [15].

Compared to dairy waste, the H_2S concentration in biogas produced at wastewater treatment plants is usually smaller, with a range of ~10–1200 ppm, as shown in Fig. 2. The actual concentrations fluctuate and depend on the liquid sanitary wastes collected and treated, and the specific treatment employed by the facility. For most cases where the concentration of H_2S is low, iron salts (such as ferrous chloride) are used in the water treatment process to remove phosphorous and H_2S as part of the local air quality management [4,17]. High concentrations of H_2S (3000 ppm) in WWTP have been reported in the literature [18], where the origin of the high sulfur concentration was found to be the soil through which the untreated water flowed between the source and the destination treatment facility. While H_2S contains the bulk of sulfur in the biogas, organic sulfur species such as mercaptans, e.g., DMS (dimethyl sulfide), are also present, although they rarely exceed 0.1 ppm.

Typically, LFG contains <100 ppm H_2S; however, the concentrations can rise to several thousand ppm in landfills with a high sulfur load. Extremely high concentrations have been measured at landfill cells where large quantities of plasterboard, wastewater sludge, or flue gas desulfurization sludge have been deposited [4]. Just as in ADG, the majority of the sulfur found in LFG is in the form of H_2S.

[1] Thermal power calculated based on LHV (lower heating value) assumes 60% methane in biogas, and 1 ft^3-biogas/100 gallon water treated (70 kWth/MGD).

[2] Efficiency of high temperature fuel cell ~45–60% (www.eere.energy.gov/hydrogenandfuelcells).

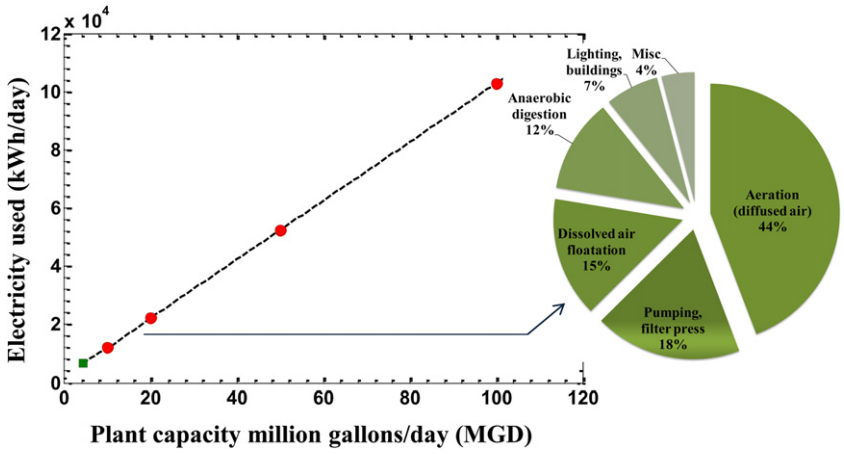

Fig. 1. Energy requirements of activated sludge treatment plants [8].

Compared to ADG, organic sulfur is found in higher concentrations in LFG. The organic sulfur is usually present as mercaptans (thiols), disulphides, and dimethyl sulfide, as shown in Fig. 3. In most cases where organic sulfur has been measured at a landfill, dimethyl sulfide was found to be present at concentrations >10 ppm.

Table 2
Impurity tolerance of AFC, PAFC, MCFC, and SOFC.

Impurity	Tolerance	Units	References
Alkaline fuel cells			
CO_2	500	ppm	[38]
Phosphoric acid fuel cells			
CO	1	%	[39]
NH_3	<1	%	[35]
H_2S	<2	ppm	[35]
Total sulfur	<4	ppm	[37]
Halogens	<4	ppm	[30,37]
Molten carbonate fuel cells			
H_2S	0.1	ppm	[30,40]
	0.5		[36]
	0.1–5		[33]
COS, CS_2, mercaptan	1	ppm	[40]
Organic sulfur	<6	ppm	[24]
H_2S, COS, CS_2	0.5–1	ppm	[32]
	<10		[24]
HCl	<0.1	ppm	[40]
Halogens (HCl)	0.1–1	ppm	[30,33,36]
Halides: HCl, HF	0.1–1	ppm	[32]
Halogenated organics	<0.1	ppm	[24]
Alkali metals	1–10	ppm	[36,40]
NH_3	1–3	%	[27,32,33,36]
NO_x	20	ppm	[33,36]
Siloxanes: HDMS, D5	<1	ppm	[24,32]
Tars	2000	ppm	[32]
Heavy metals: As, Pb, Zn, Cd, Hg	1–20	ppm	[32]
Total metals	<1	ppm	[24]
Solid oxide fuel cells			
H_2S	"Few"	ppm	[31]
	1		[30]
	<1		[4]
HCl	"Few"	ppm	[34]
NH_3	5000	ppm	[27,41]
Halogens	1	ppm	[30]
Total silicon	<0.01	ppm	[4]
Halogens	<5	ppm	[4]

Organic sulfur species react with hydrogen and carbon oxides, especially at elevated temperatures, to form H_2S and COS. Hydrogen sulfide is corrosive to the pipeline infrastructure [19], hence exposed surfaces need appropriate protection. More importantly, sulfur species deactivate catalysts in the reformer and in the fuel cell anode by reacting with the metals to form sulfides. Fuel cells that operate with high concentrations of H_2 demonstrate a higher tolerance to sulfur than those that use internal reforming of the biogas [20].

3.2. Siloxanes

Siloxanes are organic silicon compounds typically used in consumer products such as personal hygiene products, cosmetics, detergents, pharmaceuticals, and lubricants [4,21,22]. Of the hundreds of different siloxanes in use, the most commonly occurring ones in biogases are the linear species designated with the letter L (L2–L5) and cyclic species designated with the letter D (D3–D6). Compared to landfill gas, biogas from wastewater sludge digestion usually has a higher siloxane concentration, with the majority of those species consisting primarily of D4 and D5, as shown in Fig. 4. Landfill gas may contain significant quantities of other siloxanes, such as TMS (trimethylsilanol), as well. The higher siloxane content in ADG may be due to the water solubility of the compounds and also due to the increased volatilization of siloxanes

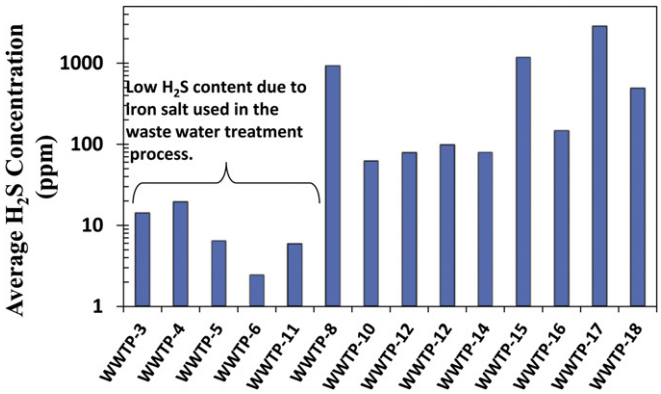

Fig. 2. H_2S concentration in digester gas from wastewater treatment plants. Excerpt from database [16].

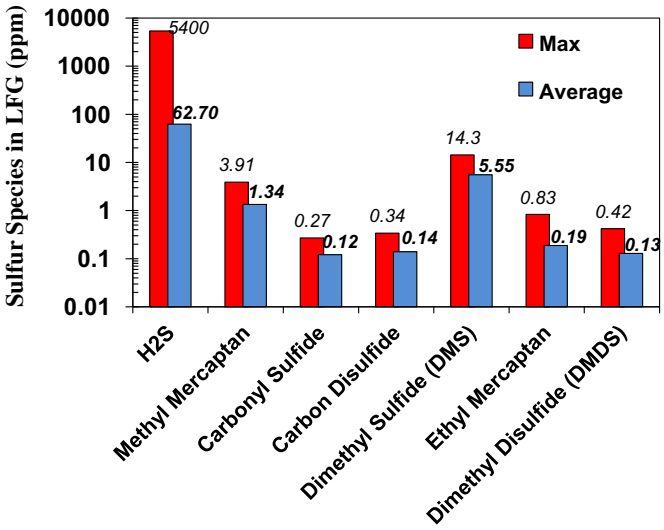

Fig. 3. Concentrations of the most frequent sulfur species measured in LFG (landfill gas). Excerpt from database [16].

caused by the elevated temperature used in the AD process. For instance, there seems to be a correlation that siloxane concentrations are higher in thermophilic digesters operating at temperature of about 55 °C than in mesophilic digesters operating at 30–35 °C [4,17,22].

Siloxanes in the fuel gas can lead to the formation and deposition of SiO_2 that can affect many components of the fuel cell system, such as heat exchangers, catalysts, and sensors [4,23,24]. Few studies have investigated the effect of siloxanes on fuel cells. Haga et al. [23] showed that 10 ppm of D5 resulted in total SOFC failure in 30 h at 1000 °C. The degradation was almost immediate at 800 °C. The failure was caused by the formation of microcrystalline silica on the anode surfaces.

3.3. Volatile organic compounds (VOCs)

Waste-derived fuels contain species such as alkanes, alcohols, aromatics and halogens. The concentrations of halogens are typically higher in landfill gas than in digester gas from wastewater treatment plants, as shown in Fig. 5. Landfill gas may contain halogenated hydrocarbons from many sources, such as discarded refrigerants, plastic foams, aerosols, paints, etc. [13]. Many of these compounds are stable and slowly evaporate to maintain significant levels of halogens in the LFG for many years [14]. Chlorine is the most abundant halogen species, while bromine- and fluorine-containing substances are generally found in smaller concentrations. The most commonly occurring fluorine compounds in LFG are CFC (chlorofluorocarbons) used in refrigerants, insulation foams, and propellants [4].

Among the hydrocarbons, paraffinic and aromatic hydrocarbons are usually found in high concentrations in LFG (Fig. 6). These species are encountered in digester gas as well, but usually at lower concentrations [25]. Among the aromatic species, benzene, toluene, and xylene are typically found at high concentrations. The concentrations of aromatics are affected by both the age (decomposition process) and the source of the waste [13,14,25]. Toluene, for example, is commonly used in making paints, lacquers, adhesives, and cosmetic products [25].

While the concentration of the hydrocarbons typically found in waste-derived fuels may not be hazardous to the fuel cell, they can greatly reduce the clean-up capacity of various adsorbents used for

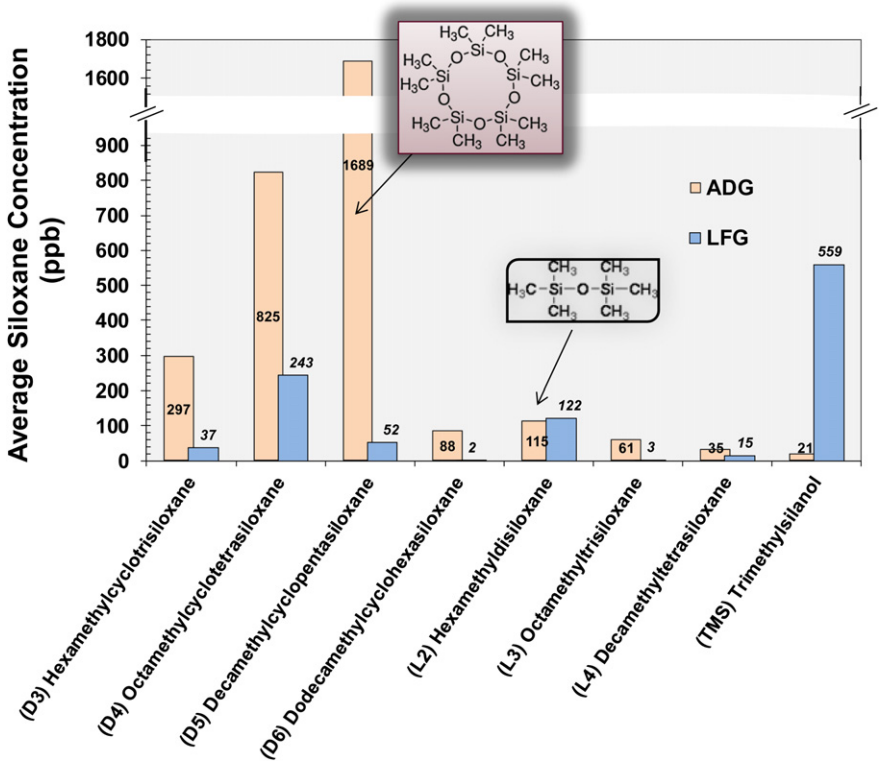

Fig. 4. Average concentrations of siloxanes measured in LFG and ADG from wastewater treatment plants. Excerpt from database [16].

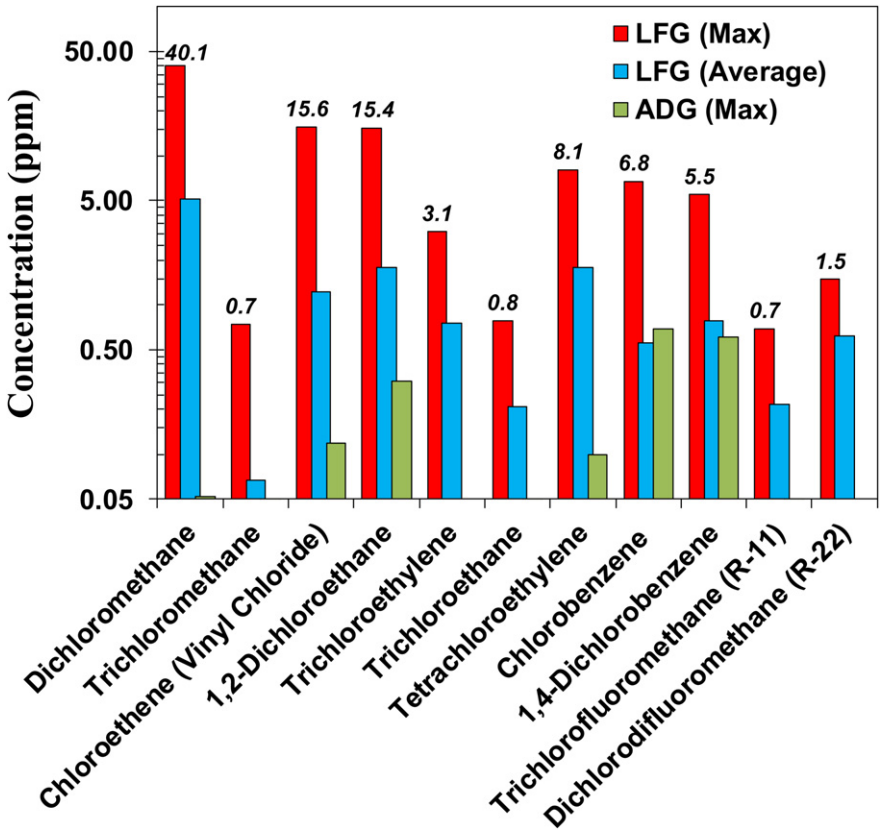

Fig. 5. Examples of typical halogenated species measured in LFG and ADG from wastewater treatment plants. Excerpt from database [16].

the removal of siloxanes [24]. Of primary concern to the fuel cell system are the halocarbons, as they convert to acid gas that can corrode catalytic surfaces [26–28]. The halogens react with the electrolyte in MCFCs (Molten Carbonate Fuel Cells) and slowly degrade the performance over time [27,29].

4. Impurity removal

The specific tolerance of a fuel cell to a given impurity is determined by the nature of the impurity and its interactions with the materials in the anode chamber, which includes the electrocatalyst and the electrolyte. The tolerance limit is defined by considerations of desired lifetime and the end-of-life power output capacity, and the trade-offs between loss in power output against the costs of impurity removal, maintenance, and process reliability. Of the various fuel cell types used in stationary installations, the impurities identified and the data sources for MCFCs are the broadest, since this type of fuel cell has been used in demonstrations using a variety of fuel feedstocks. The data summarized in Table 2 provide a glimpse at the levels of individual and class of impurities that may be allowable in the fuel gas fed to the fuel cell anode [4,24,30–41]. There is a wealth of data on the impurity effects for the PEFC (polymer electrolyte fuel cell), but the open literature reports mostly on automotive PEFCs. The PAFC (Phosphoric Acid Fuel Cell) has been widely deployed in commercial applications in the U.S. and abroad. The reports on these deployments, however, focus mainly on the application experience and performance, rather than on impurity effects.

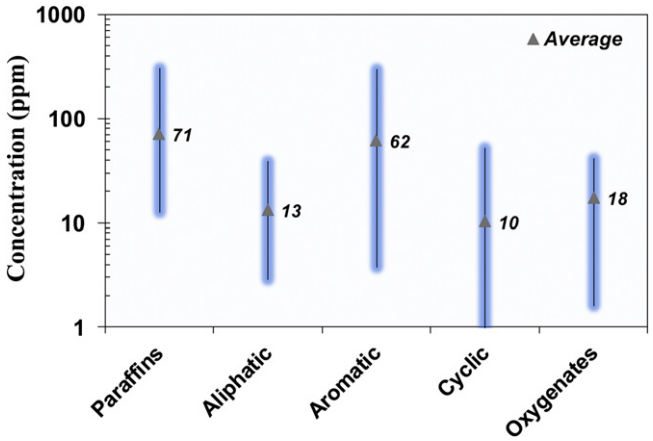

Fig. 6. Among the measured non-methane hydrocarbons, aromatic and paraffinic hydrocarbons dominate in LFG. Excerpt from database [16].

As the requirements for gas cleaning vary widely from project to project due to the variability in the source fuel gas, the processes have typically been custom engineered for each project. Thus, there are no standard solutions; rather, a specific combination of impurity removal methods is used to ensure a fuel gas of the quality that meets fuel cell tolerance defined by the manufacturer. The published literature [4,24,37,42–48] indicates that the gas clean-up strategies involve a primary clean-up, followed by a gas polishing step, before the gas is delivered to the fuel cell system.

A generic model of a stationary fuel cell-based power plant has been developed to assess the overall electrical efficiency and clean-up and maintenance costs determined by the biogas impurity matrix. The system is detailed in the sections below.

4.1. The process

As a base case system, we have considered a 300-kWe molten carbonate fuel cell system operated on digester gas from a wastewater treatment plant, which would be applicable for treatment facilities with influent rates of wastewater in the order of 10 MGD. The gas composition of the digester gas (excluding trace impurities) was assumed to be 58% CH_4, 38% CO_2 and 1% each of O_2 and N_2 on a dry basis. The gas is also saturated with water vapor at 33 °C (reflecting conditions in a mesophilic digester).

The concentrations of the trace contaminants used for this analysis are given in Table 3 as maximum and average values for both ADG and LFG. Forty-seven species were considered, distributed in 10 classes of contaminants (siloxanes, sulfur, halogens, etc.). Within each class, we included the species that occurred most frequently in the biogas, and also some other contaminants that showed particularly high concentrations (based on data from the database). The concentrations of some isomers (such as dichlorobenzene, xylene) were added together and treated as a single species. In cases where the data were too limited to determine average concentrations (as in ADG), the maximum concentration value was used.

The main GPU (gas processing unit) of the system is shown in Fig. 7. First the bulk impurity, e.g., H_2S, is removed using an appropriate technology, such as iron oxide or impregnated carbon. The gas is then cooled to remove the bulk of water vapor in the gas; and it may even be cooled to below 0 °C to condense some of the siloxanes. The gas is then passed to the secondary polishing equipment (low temperature polisher) that can contain a series of adsorbents (i.e., activated carbon, silica, zeolites) that removes organic sulfur, siloxanes, and halogens. The cleaned fuel gas is then fed to the fuel cell module, as shown in Fig. 8.

The fuel cell module includes a high temperature polisher to remove trace organic sulfur and halogenated species that are not

Table 3
Frequently occurring trace contaminants for LFG and ADG used for the analysis (excerpt from database [16]).

						LFG		ADG (WWTP)	
#	D.B. index	Class	Chemical name	Formula	Mw (g/mol)	Max (ppm)	Average (ppm)	Max (ppm)	Average (ppm)
1	2	Siloxanes	(D4) Octamethylcyclotetrasiloxane	$C_8H_{24}O_4Si_4$	296.62	0.967	0.243	20.144	0.825
2	3	Siloxanes	(D5) Decamethylcyclopentasiloxane	$C_{10}H_{30}O_5Si_5$	370.77	0.286	0.052	18.129	1.689
3	5	Siloxanes	(L2) Hexamethyldisiloxane	$C_6H_{18}OSi_2$	162.38	0.838	0.122	2.260	0.115
4	6	Siloxanes	(L3) Octamethyltrisiloxane	$C_8H_{24}O_2Si_3$	236.53	0.030	0.003	0.465	0.061
5	11	Sulfur	Hydrogen sulfide	H_2S	34.08	5400.0	62.7	2897	400
6	12	Sulfur	Methanethiol (Methyl mercaptan)	CH_4S	48.11	3.91	1.34	1.070	0.080
7	14	Sulfur	Carbon disulfide	CS_2	76.14	0.34	0.14	0.050	0.050
8	15	Sulfur	Dimethyl sulfide (DMS)	C_2H_6S	62.14	14.3	5.6	0.040	0.040
9	42	Halocarbons	Methylene chloride (Dichloromethane)	CH_2Cl_2	84.93	40.100	5.150	0.052	0.052
10	43	Halocarbons	Chloroform (Trichloromethane)	$CHCl_3$	119.38	0.743	0.067	0.009	*excl.*
11	44	Halocarbons	Carbon tetrachloride	CCl_4	153.82	0.038	0.038	0.005	*excl.*
12	45	Halocarbons	Chloroethene (Vinyl chloride)	C_2H_3Cl	62.49	15.600	1.230	0.119	0.119
13	50	Halocarbons	1,2-Dichloroethane	$C_2H_4Cl_2$	98.96	15.400	1.790	0.308	0.157
14	51	Halocarbons	Trichloroethylene	C_2HCl_3	131.39	3.100	0.755	*excl.*	*excl.*
15	53	Halocarbons	1,1,2-Trichloroethane	$C_2H_3Cl_3$	133.40	0.784	0.207	N.A.	N.A.
16	54	Halocarbons	Tetrachloroethylene	C_2Cl_4	165.83	8.060	1.780	0.100	0.100
17	60	Halocarbons	Chlorobenzene	C_6H_5Cl	112.56	6.760	0.552	0.693	0.255
18	63	Halocarbons	Dichlorobenzene (all isomers)	$C_6H_4Cl_2$	147.00	5.480	0.776	0.610	0.254
19	75	Halocarbons	Trichlorofluoromethane (R-11)	CCl_3F	137.38	0.695	0.214	0.004	0.004
20	76	Halocarbons	Chlorodifluoromethane (R-22)	$CHClF_2$	86.47	1.480	0.617	N.A.	N.A.
21	85	Alkanes	Ethane	C_2H_6	30.07	14.300	8.850	51.000	40.000
22	86	Alkanes	Propane	C_3H_8	44.09	40.000	12.100	2.000	1.000
23	88	Alkanes	Butane	C_4H_{10}	58.12	37.900	4.260	1.300	0.700
24	91	Alkanes	Pentane	C_5H_{12}	72.15	26.600	3.210	15.000	7.000
25	96	Alkanes	Hexane	C_6H_{14}	86.18	28.400	3.010	108.000	25.144
26	103	Alkanes	Heptane	C_7H_{16}	100.20	9.160	2.000	0.358	0.358
27	112	Alkanes	Octane	C_8H_{18}	114.23	33.800	4.690	0.275	0.221
28	118	Alkanes	Nonane	C_9H_{20}	128.26	32.700	6.580	6.200	1.246
29	162	Aromatic	Benzene	C_6H_6	78.11	21.300	2.170	0.850	0.168
30	163	Aromatic	Toluene (Methylbenzene)	C_7H_8	92.14	108.000	30.200	2.274	1.037
31	165	Aromatic	Ethylbenzene	C_8H_{10}	106.17	40.200	7.600	5.911	1.251
32	166	Aromatic	Xylenes (o-, m-, p-, mixtures)	C_8H_{10}	106.17	108.000	10.600	4.095	0.784
33	172	Aromatic	1,3,5-Trimethylbenzene	C_9H_{12}	120.19	10.390	3.849	1.859	1.859
34	182	Aromatic	1-Methyl-4-propylbenzene (p-cymene)	$C_{10}H_{14}$	134.22	8.050	3.380	3.072	1.157
35	201	Cyclic	Cyclohexane	C_6H_{12}	84.16	3.360	1.120	*excl.*	*excl.*
36	205	Cyclic	Methylcyclohexane	C_7H_{14}	98.19	11.500	2.840	0.130	0.130
37	208	Cyclic	Dimethylcyclohexane (all isomers)	C_8H_{16}	112.21	34.660	5.275	0.390	0.390
38	224	Cyclic	Limonene	$C_{10}H_{16}$	136.23	35.380	11.948	48.900	9.729
39	227	Alcohol	Ethanol	C_2H_6O	46.07	0.394	0.222	N.A.	N.A.
40	229	Alcohol	2-Propanol (Isopropyl alcohol)	C_3H_8O	60.10	6.630	1.920	N.A.	N.A.
41	237	Ester	Ethyl acetate	$C_4H_8O_2$	88.11	4.600	1.810	N.A.	N.A.
42	242	Ester	Ethyl butanoate (Butanoic acid)	$C_6H_{12}O_2$	116.16	1.997	1.997	N.A.	N.A.
43	251	Ether	Dimethyl ether	C_2H_6O	46.07	0.632	0.632	N.A.	N.A.
44	253	Ether	2-methoxy-2-methyl-propane (MTBE)	$C_5H_{12}O$	88.15	0.257	0.106	N.A.	N.A.
45	254	Ketone	Acetone	C_3H_6O	58.08	15.500	6.820	N.A.	N.A.
46	255	Ketone	2-Butanone (Methyl ethyl ketone)	C_4H_8O	72.11	9.430	4.070	N.A.	N.A.
47	257	Ketone	4-Methyl-2-pentanone (MIBK)	$C_6H_{12}O$	100.16	2.170	0.840	N.A.	N.A.

excl: species excluded in the analysis due to particular low concentration within the same group.
N.A.: data not available, D.B. = database index.

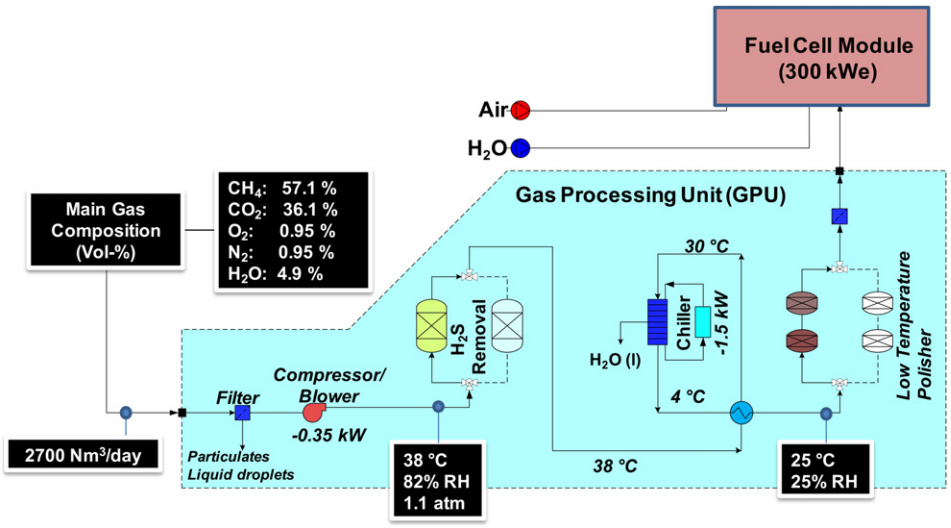

Fig. 7. Process model of the GPU (gas processing unit) for a molten carbonate fuel cell system operating on anaerobic digester gas.

captured by the gas processing unit [49–51]. The hydrogen needed for the HDS (hydro-desulfurizing unit) is obtained by recycling a slip-stream (6%) from the anode tail gas. This anode slip-stream is first cooled to 60 °C, to condense out the bulk of the water and increase the hydrogen concentration, before it is mixed with the fuel from the GPU. The fuel gas mixture is compressed to ~25 psia and heated to 330 °C before entering the high temperature polisher. The cleaned gas is mixed with steam (steam-to-carbon ratio of 2.5) and fed to a pre-reformer, where the fuel is partially reformed at a temperature of 440 °C before entering the fuel cell stack.

For the fuel cell, we have used a model similar to that developed by Lukas et al. [52,53]. The model discretizes the stack into 40 well stirred control volumes for both the anode and cathode, and it assumes that the temperature is equal within each control volume. The model accounts for the internal reforming reactions and fuel cell irreversible losses contributed by activation, concentration, and ohmic polarizations. The partially reformed fuel enters the anode where it is further internally reformed via SMR (steam methane reforming), Eq. (1), and the WGS (water gas shift) reaction, Eq. (2), to hydrogen. The hydrogen reacts by the anode half-cell electrochemical reaction Eq. (3). For the SMR reaction, we used the

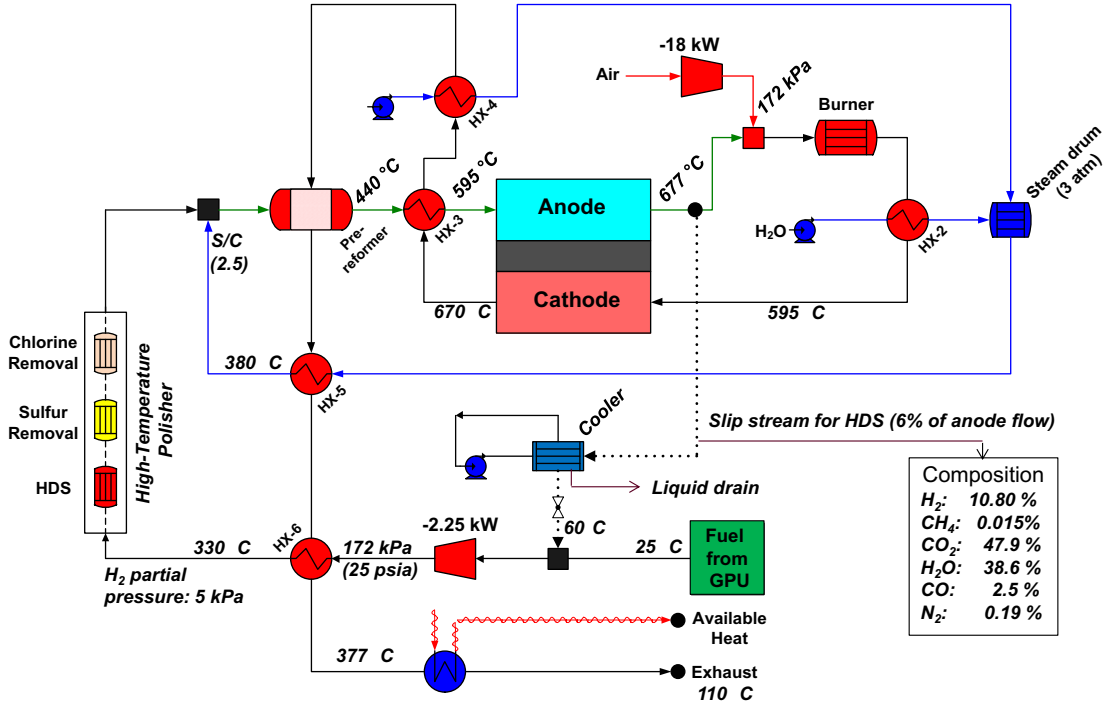

Fig. 8. Process model of the fuel cell module including the stack (300 kW MCFC), BOP (balance of plant), and high temperature polisher.

kinetics used by Lukas et al. [53]. It was assumed that the WGS reaction is equilibrium limited. Only hydrogen participates in the electrochemical reaction.

Methane steam reforming

$$CH_4 + 2H_2O \Leftrightarrow CO + 3H_2 \quad (1)$$

Water gas shift

$$CO + H_2O \Leftrightarrow CO_2 + H_2 \quad (2)$$

Anode half-cell electrochemical reaction

$$H_2 + CO_3^{2-} \Rightarrow H_2O + CO_2 + 2e^- \quad (3)$$

The anode tail gas is fed to the burner and recycled to the cathode where the following electrochemical reaction takes place, Eq. (4).

Cathode half-cell electrochemical reaction

$$CO_2 + \frac{1}{2}O_2 + 2e^- \Rightarrow CO_3^{2-} \quad (4)$$

The cathode effluent, after passing a series of heat exchangers (i.e., for anode gas pre-heating, steam generation), enters the heat recovery unit at ~380 °C (~710 °F) and leaves the system as waste heat at 110 °C. The recovered heat can be used by the water treatment plant to meet the energy needs of the anaerobic digestion process and for space heating where needed. Given the assumptions for the process shown in Table 4, a net electrical efficiency of 47% and a total CHP efficiency of 69.5% based on the fuel (biogas) LHV was calculated. This value corresponds closely to the efficiencies reported for MCFC demonstration projects operated on anaerobic digester gas and in the manufacturer's data [42].

4.2. Primary clean-up (H_2S)

The first step in the clean-up system in the GPU was the removal of the hydrogen sulfide. Iron oxide media (SulfaTreatHP®) was selected for its removal in this analysis. Desulfurization is achieved by reaction with mixed-metal oxides forming a stable metal sulfide. There are many similar media options for H_2S removal, such as impregnated activated carbon [54–57], and other proprietary iron oxide media, such as Sulfur-Rite®, Sulfa-Bind®, and Iron Sponge, as well. Part of the reason for choosing SulfaTreat® was that information in case studies [42,45] and in the literature [58] were helpful in developing a model for design purposes and qualitatively asses the adsorption capacity as a function of inlet concentration and bed volumes.

Table 4
Operating conditions and system efficiencies for the 300 kWe MCFC plant.

Characteristics	Value	Units
Fuel cell		
Fuel utilization	70	%
Oxygen utilization	40	%
Voltage	767	mV
Current density	137	mA/cm^2
DC/AC efficiency	98	%
Pressure	137	kPa
Balance of plant		
Parasitic power (GPU + Fuel cell plant)	22.3	kW
Compressor/blower efficiency	78	%
Heat loss – heat exchanger	8	% of heat load
Heat loss – Burner	10	% of anode LHV
Heat loss – Fuel cell	1.8	% of fuel LHV
Efficiencies		
Net electrical efficiency	47	% of fuel LHV
Total CHP efficiency	69.5	% of fuel LHV

The model, Eq. (5), considers the transient behavior of a packed bed filled with spherical particles. It is a two-phase model accounting for the gas phase as well as the solid phase. The equation for the particle assumes diffusion as the rate limiting step, and it is derived from the principles of the shrinking core model [59,60]. The model and assumptions are summarized in the supplemental material and all symbols are explained in notation

$$\left.\begin{aligned} \varepsilon_b \frac{\partial C}{\partial t} &= D_L \frac{\partial^2 C}{\partial x^2} - U_0 \frac{\partial C}{\partial x} - \sigma k_f C \left(1 - \frac{k_f R_0 (1 - R/R_0)}{D_e R/R_0 + k_f R_0 (1 - R/R_0)}\right) \\ &\text{Particle equation} \\ \frac{dR}{dt} &= -\frac{D_e C}{C_B} \left(\frac{k_f R_0 (1 - R/R_0)}{D_e R/R_0 + k_f R_0 (1 - R/R_0)}\right) \left(\frac{1}{R - \frac{R^2}{R_0}}\right) \end{aligned}\right\} \quad (5)$$

Truong et al. [58] performed a characterization of SulfaTreat® at lab-scale conditions. The maximum adsorption capacity of sulfur (g-S/g-adsorbent) was estimated to be 12 wt%. From breakthrough experiments, the results indicated that the diffusion and the surface reaction rates are of the same order of magnitude and that the gas must be saturated in water to give optimum results. With one adjustable parameter, D_e, the model could be fitted to the breakthrough data by Truong et al. [58] (see Fig. 9a) and could also predict other experimental conditions such as change in contact time (variations in bed length). However, as those experiments were done at 20 °C, the reaction rate is low and the oxide media performs poorly (only 2.8 wt% adsorption capacity of sulfur was achieved when H_2S was detected in the effluent gas).

In tests done at the Anoka Landfill with SulfaTreat®, low temperatures (below 38 °C) was the cause of early breakthrough of H_2S detected at the exit of the bed [45]. Once the bed was heated the H_2S dropped again to levels below detection limit (100 ppb). Unfortunately, the size of the beds was not disclosed in that report to further calibrate the model. However, the information was useful in that the operating parameters (temperature) appear to be very important in achieving a high adsorption capacity (and likely attain pore diffusion control). Furthermore, while the inlet concentration of H_2S varied between 60 and 100 ppm, the iron oxide media effectively reduced the concentration to below 0.1 ppm (detection limit). Methyl mercaptan was removed completely as well, corroborating manufacturer information that iron oxide media is effective for the removal of mercaptans. The iron oxide media was ineffective in removing DMS (dimethyl sulfide), however [45].

The model was calibrated with the data from the King County Case Study [42], using breakthrough times projected by the vendor from the flows and bed sizes used in the process (shown in Fig. 9b). The diffusivity rate was increased by a factor of 4 (to 3×10^{-8} m^2/s) in comparison to the data by Truong et al. [58] and the adsorbent utilization increased from 2.5 to 6.8 wt%.

The "breakthrough concentration" is defined as the concentration of the impurity in the bed effluent when the bed is considered to have reached its capacity. This value is usually a percentage of the inlet concentration of the species, and it is selected by the design engineer. Defining a higher breakthrough concentration of H_2S allows greater utilization of the sulfur sorption capacity. If only one vessel is used (and no other means to remove H_2S are used after this treatment step) assigning a low breakthrough concentration (e.g., 0.1 ppm) would underutilize the

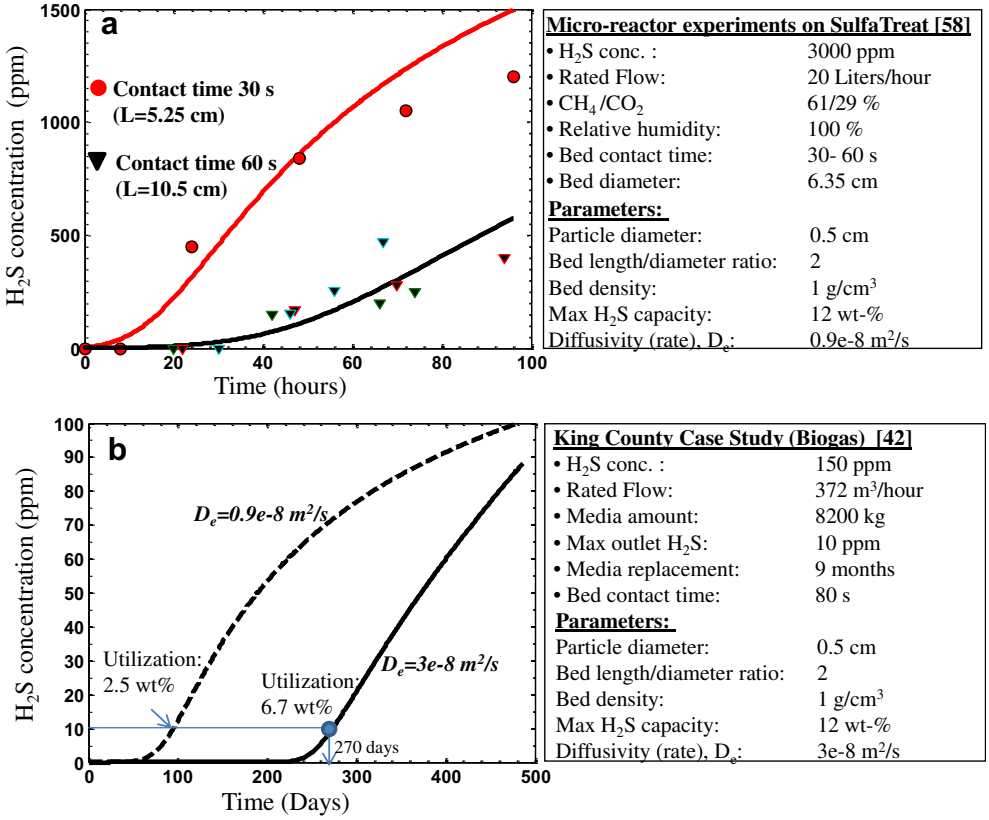

Fig. 9. (a) Comparison of shrinking core model with H_2S breakthrough data by Truong et al. [58] on SulfaTreat. Symbols = experimental data, line = model. (b) Effect of diffusivity on expected breakthrough capacity for the King-County demonstration project [42].

sorbent. It is common to have two vessels operated in series (called lead and lag configuration). When the lead vessel reaches the breakthrough concentration the flow is switched to make the second vessel the lead vessel, while the lag vessel is refilled with fresh media and made the new lag vessel. This lead and lag configuration can be viewed as a safety net to account for variations in operating conditions (such as temperature and the inlet concentration of the contaminant).

Some of the iron oxide bed design parameters (base case) and assumptions used in the analysis are as follows:

- Contact time: 60–120 s
- 2-vessel design (equal bed volumes), lead and lag configuration
- Lead vessel breakthrough concentration of H_2S: 15 ppm
- Temperature: 38 °C (fast kinetics – pore diffusion control)
- All H_2S and mercaptans are removed. All other organic sulfur is assumed to breakthrough continuously.

4.3. Gas drying (by cooling/condensation)

The gas from the sulfur removal beds needs to be dried before entering the polisher. Moisture, especially at RHs (relative humidities) exceeding 40%, can significantly reduce the capacity of adsorbents like activated carbon [61–65]. Other adsorbents such as silica gel and zeolites are even more sensitive to moisture and may require the gas to be almost dry (RH < 10%) [24,66]. For our base case, we have considered activated carbon as the adsorbent media (Section 4.4) and have assumed that an RH of ≤25% has a negligible effect on the adsorption capacity of the sorbent.

After the bulk sulfur removal, the gas is passed through a chiller/condenser that cools the gas to a dew point of 4 °C. After removal of the condensed water in a knock-out tank, the gas is reheated to 25 °C (RH = 25%) in a heat exchanger by using the warm biogas stream exiting the H_2S removal bed (Fig. 7). The refrigeration cycle was calculated using the software Duprex 3.2 with Suva™ 134a as the refrigerant.

At a temperature of 4 °C, only water condensed out leaving all the trace impurities in the gas phase (based on vapor pressure), even in cases where the maximum concentration values were used (both for LFG and ADG). Some removal of VOCs after condensing out the water has been observed in some cases [66]. This may be the result of some of the soluble species such as alcohols dissolving out with the condensed water. Cooling is not sufficient to ensure condensation of the higher hydrocarbons in the concentrations that they are present in the biogas matrix (even after cooling to 0 °C). The only species that were predicted to condense out by cooling (vapor pressure data) are cyclic siloxanes, especially D5 [67]. At low concentrations (1 ppm) and pressures (1 atm), condensation of D5 starts at temperatures below −35 °C. At this temperature, if the concentration of D5 is 10 ppm, almost 90% would be removed. Increasing the pressure increases the condensation temperature; for example, at 5 atm and for inlet concentration of 10 ppm, the condensation would start at ~2 °C and 90% could be removed at ~20 °C.

While chilling to below 0 °C in combination with high pressures can be effective for some siloxanes, linear siloxanes (such as L2) having higher vapor pressure are likely to remain in the gas phase at high concentrations even after chilling [67]. Furthermore, the requirement of low temperatures and high pressures adds to

capital cost and increased power consumption, and such a strategy may be advisable only in cases with extremely high concentrations of siloxanes (in particular D5). In the base case, with typical concentration of D5 in the range of 1–5 ppm (average concentration of 1.7 ppm), the gas was only dried by cooling to 4 °C. The remaining trace impurities were removed in subsequent steps.

Some of the base case design parameters and assumptions for the chiller/condenser are as follows:

- Dew point: 4 °C
- RH at 25 °C: 25%
- No trace impurities are condensed/washed out
- COP (coefficient of performance) for refrigeration cycle: 3.4.

4.4. Low temperature polisher (activated carbon)

AC (Activated carbon) is frequently used for the removal of organic vapors [68–70], and it has also been demonstrated to be efficient in removing siloxanes [66,71,72]. AC is defined here as carbon that has not been impregnated (such as KOH-impregnated carbon) or functionalized by, for example, Cu or Cr. Impregnated or functionalized carbons are used to target specific impurities such as H_2S or organic sulfur. In this analysis, H_2S is removed using an iron oxide bed (discussed earlier), and AC is considered for the first step of the polisher to estimate the effectiveness for removing the trace contaminant matrix as given in Table 3.

The service life of the carbon depends on the operating parameters (such as temperature and pressure) and by the adsorption affinity of the carbon for the individual species. To properly address the adsorption capacity and the corresponding operating costs of the carbon bed, adsorption data are needed as a function of concentration and temperature for each contaminant species of interest. Furthermore, the adsorption capacity for each adsorbate is greatly influenced by the other species in the mixture. Aromatic compounds, for instance, will strongly adsorb on carbon and displace many halogenated compounds and siloxanes leading to their early breakthrough. Therefore, the composition of the mixture is important in determining the service life of the bed. The model includes these effects to estimate the breakthrough for each species in a bed filled with activated carbon. The model is briefly outlined below.

4.4.1. Adsorption isotherms

The Dubinin–Radushkevich (D–R) equation [73] was used to determine the adsorption isotherms (q) for all species given in Table 3. We have used the correlation proposed by Ye et al. [70]:

$$\left(\frac{k_v q V_b}{V_0}\right) = -\left(\frac{P/P_v}{\beta E_0}\right) \tag{6}$$

$$E_0 = \frac{2872}{T} \tag{7}$$

where the symbols are explained in notation. Some of the parameters can be readily obtained; the vapor pressure (P_v) and liquid molar volume (V_b) can be obtained from thermodynamic properties [74], and the adsorption volume (V_o) from the carbon manufacturer or by measurement. The affinity coefficient (β) and the pore volume adjusting coefficient (k_v) are parameters that need to be estimated [75] or fitted to adsorption isotherm data. For the most part, we could find literature data for many of the species shown in Table 3 and fit Eq. (6) to those data [56,61,62,70,75–91]. For the cases where data were not available (8 species), the parameters were correlated by using a reference species of similar properties and the method developed by Ye et al. [70]. The set of coefficients (β and k_v) to model the isotherm with Eq. (6) are given in Table 5.

Fig. 10 shows the adsorption capacity (as weight fraction) of activated carbon on some select impurities. The lines are modeled adsorption isotherms on pure organic components and the symbols are experimental data from the literature. Hydrogen sulfide, for instance, has a rather low adsorption capacity on activated carbon and consequently needs specific media for its removal (i.e., iron oxides or KOH-impregnated carbon).

Other species, such as chlorobenzene and aromatics (toluene), show very high adsorption capacities, even at low partial pressures.

4.4.2. Estimating breakthrough for multiple species

Once the adsorption isotherms for each individual species are established, the adsorption capacity is then determined in the mixture. The IAST (ideal adsorbed solution theory) was used to predict multicomponent adsorption equilibria [85]. The expanding zone model by Wood and Snyder [92] was used in this study to predict multicomponent breakthrough times for each vapor in the carbon bed. Details regarding the model are given in Ref. [92] and references therein. Briefly, the movement of the vapors in the bed is idealized to occur in distinct zones. At a finite time, the first zone (near the entrance of the bed) contains all vapors. At some further distance into the bed, all but the strongest adsorbed vapor pass into zone 2. This process continues until one vapor remains in the last zone. The widths of the zones expand with time until they reach the end of the bed; this both because of the inlet flow to the bed and also due to competitive adsorption. As a zone expands, the vapors already adsorbed in subsequent zones may be displaced by the more strongly adsorbed vapors (concentration roll-up).

The expanding zone model was compared with data in the literature for multicomponent mixtures. Shin et al. [61] measured the breakthrough time for 8 species in raw landfill gas using activated carbon. Fig. 11 shows the comparison between the experimental data and the model for some of those species. The broken lines are the calculated concentration profiles at the exit of the bed as a function of time. The model assumes infinite kinetics (no mass-transfer) and the concentration profile is consequently flat (square wavefronts) as opposed to the experimental stretched “S” shapes. Overall, the stoichiometric breakthrough times (50% of inlet concentration) and the order of breakthrough are predicted reasonably well as well as the magnitude of the concentration roll-up. Once the equilibrium capacities are determined for each zone kinetics can be incorporated to mimic the observed S-shapes [92]. Rate coefficients were calculated using the Wood–Lodewyckx correlation for when the outlet concentration reached 1% of the vapor’s inlet concentration, see Wood and Snyder [92] for details. Skew corrections and corrections factor on elution order were neglected.

4.4.3. Activated carbon effectiveness—ADG

For a flow rate of 2700 Nm^3/day, a single bed filled with 700 kg of activated carbon was used to calculate the breakthrough of the ADG impurity matrix (average concentrations as shown in Table 3). The properties of activated carbon used in the analysis were based on that of Calgon BPL with a micropore volume of 0.42 cm^3/g, BET surface area of 1050 m^2/g, and a bulk density of 450 kg/m^3. In addition to the trace contaminants, the adsorption effects for CH_4 and CO_2 on activated carbon were also included, based on their Langmuir isotherms [93]. Fig. 12a shows the breakthrough time (days) for some of the species that are adsorbed strongly in the bed for the ADG composition. The value in

Table 5
Affinity (β) and volume adjusting (k_v) coefficients for the Dubinin–Radushkevich (D–R) adsorption isotherm. Coefficients calibrated with experimental data (and specific carbon) were recalculated for BPL activated carbon ($V_0 = 0.42$ cm^3/g). Correlated isotherms used the reference species as denoted in the parenthesis (species #).

#	Class	Chemical name	Formula	Exp. Data/Correlation	Carbon	β	k_v
1	Siloxanes	(D4) Octamethylcyclotetrasiloxane	$C_8H_{24}O_4Si_4$	[77,91]	B1/NC60	0.67	0.70
2	Siloxanes	(D5) Decamethylcyclopentasiloxane	$C_{10}H_{30}O_5Si_5$	Correlated (1)	BPL	0.81	0.70
3	Siloxanes	(L2) Hexamethyldisiloxane	$C_6H_{18}OSi_2$	[91]	NC60	1.20	0.65
4	Siloxanes	(L3) Octamethyltrisiloxane	$C_8H_{24}O_2Si_3$	Correlated (3)	BPL	1.60	0.70
5	Sulfur	Hydrogen sulfide	H_2S	[56]	RB1	0.47	1.90
6	Sulfur	Methanethiol (Methyl mercaptan)	CH_4S	[79]	BPL	0.45	2.20
7	Sulfur	Carbon disulfide	CS_2	[79]	BPL	0.63	1.20
8	Sulfur	Dimethyl sulfide (DMS)	C_2H_6S	[79]	BPL	0.60	1.20
9	Halocarbons	Methylene chloride	CH_2Cl_2	[80]	BPL	0.52	1.10
10	Halocarbons	Chloroform (Trichloromethane)	$CHCl_3$	[78]	BPL	0.72	1.05
11	Halocarbons	Carbon tetrachloride	CCl_4	[80]	BPL	0.58	0.92
12	Halocarbons	Chloroethene (Vinyl chloride)	C_2H_3Cl	[85]	PCB	0.72	1.00
13	Halocarbons	1,2-Dichloroethane	$C_2H_4Cl_2$	[88]	U03	0.60	1.00
14	Halocarbons	Trichloroethylene	C_2HCl_3	[80]	BPL	0.78	1.00
15	Halocarbons	1,1,2-Trichloroethane	$C_2H_3Cl_3$	[80]	BAC	0.64	0.92
16	Halocarbons	Tetrachloroethylene	C_2Cl_4	[84]	U03	0.96	1.00
17	Halocarbons	Chlorobenzene	C_6H_5Cl	[81]	G209	0.84	1.00
18	Halocarbons	1,4-Dichlorobenzene	$C_6H_4Cl_2$	[76]	BPL	0.90	1.10
19	Halocarbons	Trichlorofluoromethane (R-11)	CCl_3F	[83]	BPL	0.70	0.92
20	Halocarbons	Chlorodifluoromethane (R-22)	$CHClF_2$	[83]	BPL	0.57	1.38
21	Alkanes	Ethane	C_2H_6	[87]	BPL	0.52	1.52
22	Alkanes	Propane	C_3H_8	[82]	BPL	0.62	1.15
23	Alkanes	Butane	C_4H_{10}	[82]	BPL	0.77	1.08
24	Alkanes	Pentane	C_5H_{12}	[86]	BPL	0.89	1.03
25	Alkanes	Hexane	C_6H_{14}	[62]	BPL	1.00	0.92
26	Alkanes	Heptane	C_7H_{16}	[75]	BPL	1.18	0.92
27	Alkanes	Octane	C_8H_{18}	[75]	BPL	1.24	0.97
28	Alkanes	Nonane	C_9H_{20}	[75]	BPL	1.40	1.00
29	Aromatic	Benzene	C_6H_6	[80]	BPL	0.80	0.92
30	Aromatic	Toluene (Methylbenzene)	C_7H_8	[80]	BPL	1.00	0.92
31	Aromatic	Ethylbenzene	C_8H_{10}	Correlated (25)	BPL	1.10	1.40
32	Aromatic	Xylenes (o-, m-, p-, mixtures)	C_8H_{10}	[90]	Y-20	1.10	0.88
33	Aromatic	1,3,5-Trimethylbenzene	C_9H_{12}	Correlated (25)	BPL	1.13	1.00
34	Aromatic	1-Methyl-4-propylbenzene	$C_{10}H_{14}$	Correlated (25)	BPL	1.22	1.00
35	Cyclic	Cyclohexane	C_6H_{12}	[75]	BPL	0.80	1.00
36	Cyclic	Methylcyclohexane	C_7H_{14}	Correlated (25)	BPL	1.00	1.00
37	Cyclic	Dimethylcyclohexane	C_8H_{16}	Correlated (25)	BPL	1.10	0.98
38	Cyclic	Limonene	$C_{10}H_{16}$	Correlated (25)	BPL	1.24	0.97
39	Alcohol	Ethanol	C_2H_6O	[89]	BPL	0.52	1.30
40	Alcohol	2-Propanol (Isopropyl alcohol)	C_3H_8O	[89]	BPL	0.64	1.04
41	Ester	Ethyl acetate	$C_4H_8O_2$	Correlated (40)	BPL	0.83	1.05
42	Ester	Ethyl butanoate (Butanoic acid)	$C_6H_{12}O_2$	Correlated (40)	BPL	1.06	1.00
43	Ether	Dimethyl ether	C_2H_6O	[70]	BPL	0.63	1.52
44	Ether	2-methoxy-2-methyl-propane	$C_5H_{12}O$	[70]	BPL	0.88	0.93
45	Ketone	Acetone	C_3H_6O	[80]	BPL	0.64	1.15
46	Ketone	2-Butanone (Methyl ethyl ketone)	C_4H_8O	[70]	BPL	0.76	0.90
47	Ketone	4-Methyl-2-pentanone (MIBK)	$C_6H_{12}O$	[70]	BPL	1.04	1.03

parentheses after each species denotes the inlet concentration in ppm. Most of those species are aromatics, terpenes (limonene), and high molecular weight hydrocarbons, such as nonane and octane. Some halogenated species (e.g., dichlorobenzene) and the linear siloxanes (e.g., L2) appear to have a strong adsorption affinity on carbon. L3 was predicted to adsorb much stronger than L2 and was not included in the analysis (the concentration of L3 was added to L2).

Fig. 12b shows the other side of the species spectrum – species that breakthrough early. Most low molecular weight hydrocarbons, such as ethane and propane, do not adsorb well on carbon and breakthrough the bed almost immediately. Species of concern to the fuel cell that leave the bed very early (~5 days) are dimethyl sulfide and methylene chloride. The next groups of species with early breakthrough are vinyl chloride < carbon disulfide < trichloro-fluoromethane, with an estimated breakthrough time of about 30 days. The first siloxane species that was observed to elute the bed is D4 with an approximate breakthrough time of 165 days, followed by D5 (173 days). Experimental data on siloxane uptake at breakthrough for L2 and D5 confirm a stronger adsorption affinity for L2 [66]. The order of elution of the cyclic siloxanes agrees with the study by Matsui et al. [71]. The authors determined the breakthrough for two siloxanes (D4 and D5) in a mixture of digester gas from a wastewater treatment plant. D4 followed by D5 were the first species to elute the bed. The authors measured the inlet and outlet composition of the siloxanes but did not specify the composition for the rest of the biogas.

Since siloxanes are of particular concern for fuel cell systems [4,23,24], a reasonable replacement period for the carbon would be either before dichloroethane breaks through (81 days) or just before the first siloxane, D4, breaks through (~165 days). Dichloroethane adds ~50% out of the total chlorine concentration (370 ppb), if that species is not captured by the bed (note that there are 2 chlorine atoms per molecule). The total concentration for the chlorine added by dichloroethane is too small to justify more frequent carbon media replacement (81 days as opposed to 165 days for D4). The replacement period for the carbon bed was based

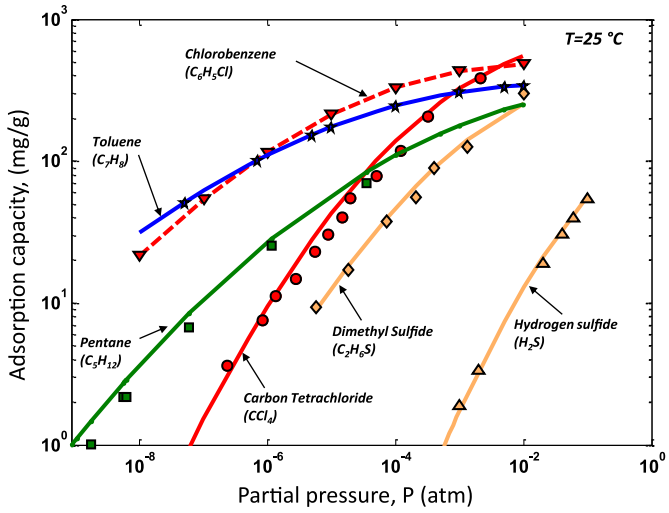

Fig. 10. Adsorption isotherms on activated carbon (BPL) on some of the most frequent encountered trace impurities in digester gas. Solids are modeled pure component isotherms and symbols corresponding experimental data from the literature.

on D4 capture (limiting species for the media). This service life of ~165 days is also influenced by operating parameters and variations in ADG composition.

The sensitivity of some of those parameters to the service life of the media is shown in Fig. 13. By increasing the pressure, the breakthrough time for D4 decreases. This seems counterintuitive at first, since the adsorption capacity increases with partial pressure (see isotherms in Fig. 10). This is true for some species, particularly if their adsorption capacity increases steeply with pressure. However, the other effect of pressure is that it also increases the competition of adsorption space, in particular due to CH_4 and CO_2. While CO_2 and CH_4 do not adsorb on carbon as strongly as VOC, the combination of high concentrations and high pressure will favor their adsorption on the carbon and, thus, reduce the ability of the bed to trap D4.

Temperature is an important operating parameter and strongly affects the adsorption capacity for all species. Decreasing the temperature to 10 °C will increase the service life of the bed, provided that the relative humidity remains low. However, if the chiller operates at a dew point of 4 °C (base case) the relative humidity will be 66% and this will greatly increase the adsorption of water vapor on the carbon [63,64]. The benefit (higher adsorption capacity for the VOCs and siloxanes) of lower temperature operation is realizable only if the moisture content is lowered before the carbon bed. To gain this benefit will require a different drying strategy, such as chilling below 0 °C or using drying media (e.g., silica). This will likely increase the complexity and cost of the system. On a final note, the proper weatherization is important for the carbon beds, especially when operating in colder climates. The bed operating temperature needs to be maintained at or above 25 °C to avoid moisture adsorption and even condensation of water in the beds.

The concentration of the halogens in ADG is low, and the majority of those species adsorb less strongly than D4. Hence,

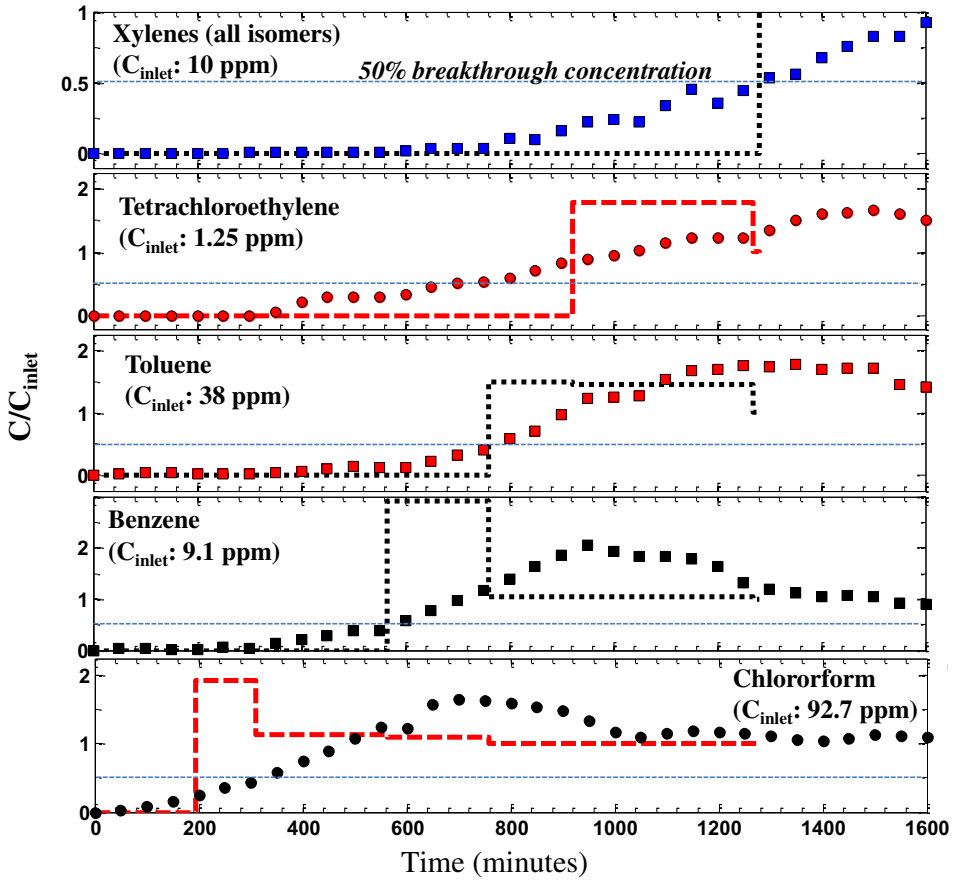

Fig. 11. Comparison of breakthrough curves using the zone model (broken lines) with experimental data (symbols) on landfill gas [61].

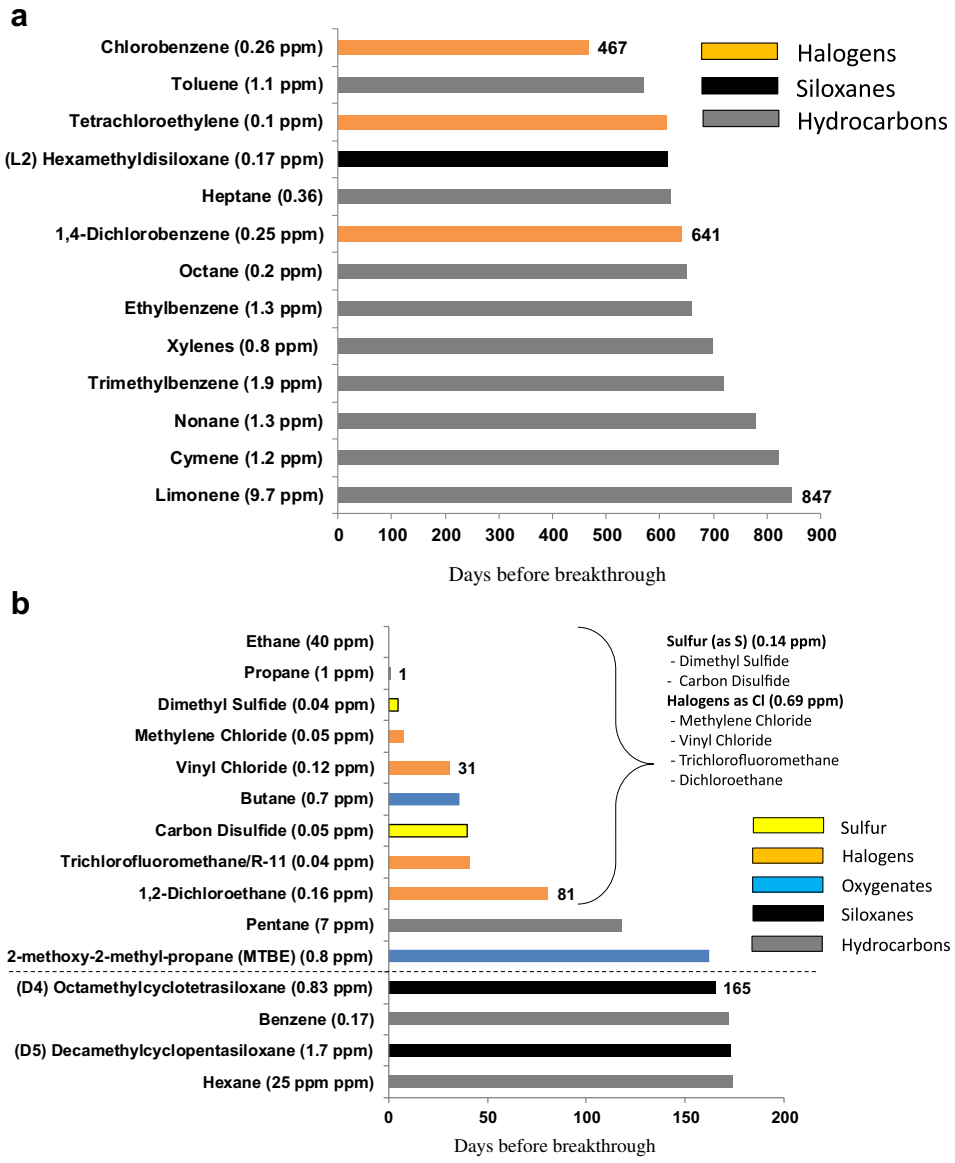

Fig. 12. (a) Breakthrough time for strongly adsorbed species on activated carbon (average ADG composition). (b) Breakthrough time for weakly adsorbed species on activated carbon (average ADG composition).

variations in the concentrations of halogens have little effect on the breakthrough time for D4. On the other hand, variation of concentrations of other contaminant groups has greater impact on breakthrough times. Among the alkanes, hexane has the greatest effect on the adsorption capacity for D4 whereas other alkanes, such as ethane or propane, that have negligible adsorption affinity for carbon, do not affect the breakthrough time for D4.

Higher concentrations of siloxanes increase the replacement frequency for the bed. When the concentration is increased to 5.3 ppm, the breakthrough time for D4 is reduced by 13% to 142 days. For average and moderately high siloxane concentrations, activated carbon appears to be effective for the adsorption of siloxane without the need for deep chilling.

Some of the base case design parameters and assumptions for the carbon bed are as follows:

- Pressure: 1.1 atm
- Temperature: 25 °C
- Moisture at RH = 25% does not affect the adsorption capacity of AC
- Carbon media: Calgon BPL (700 kg per bed/2 beds in series in lead and lag configuration)
- Bed replacement: ~165 days (D4 is the limiting species).

4.4.4. Activated carbon effectiveness—LFG

For comparison, the service life of the carbon beds was calculated for the average LFG (landfill gas) composition (Table 3). The gas contained 50% CH_4, 48% CO_2, and 1% each of O_2 and N_2 on a dry basis. Fig. 14 shows the breakthrough times for the species that have the lowest adsorption capacity. Similar to the ADG case, D4 is the first siloxane to breakthrough. However, due to adsorption competition, in particular due to the higher concentrations of hydrocarbons in landfill gas, the breakthrough time for D4 is reduced to 122 days. Landfill gas may contain high concentrations of TMS (trimethylsilanol) but the species was excluded from the

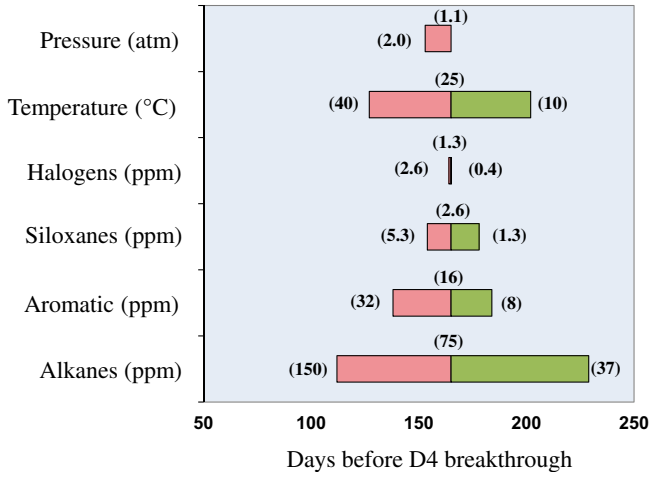

Fig. 13. Sensitivity of D4 breakthrough time to operating parameters and concentration. The concentration for each species within a class of impurities (e.g., halogens) was either doubled or reduced by half from the average ADG composition.

analysis as adsorption data for TMS were not found in the literature. Thermodynamic properties for TMS were significantly different from those for other siloxane species and we had no confidence to correlate the adsorption isotherm of TMS to a similar reference species.

The concentration of halogens and sulfur that breakthrough before D4 is substantially higher in LFG than ADG. The total concentration of sulfur (excluding H_2S and mercaptans) and halogens (as chlorine atom basis) in the influent gas is 7.2 and 28.8 ppm respectively. Basing the service life of the carbon beds before D4 breaks through (~122 days), the total cumulative chlorine concentration in the effluent gas would add up to ~18 ppm. Already after 5 days of operation, DMS alone accounts for the majority of sulfur (5.6 ppm) exiting the bed and methylene chloride for ~40% (12.1 ppm) of the total halogen content in LFG.

4.5. High temperature polisher

For a service life of AC determined by D4, most of the organic sulfur and some halogenated species will not be adsorbed by the bed. In the case of ADG, where the concentrations of the organic sulfur and halogens are relatively low, if the fuel cell can tolerate these low levels and the raw ADG is not prone to sudden spikes in these species, the gas can be fed directly to the fuel cell. With LFG, however, where the DMS (dimethyl sulfide) and methylene chloride add up to 6 ppm of sulfur and 12 ppm of chlorine (on average), an activated carbon guard bed is highly desirable.

Finding effective methods to remove DMS and, in particular, halogens, such as methylene chloride and vinyl chloride, at close to ambient temperatures proved difficult with published technology. For DMS, there are few adsorbents such as Cu-impregnated carbons and zeolites (Zeolite 13X) that can achieve adsorption capacities for sulfur of ~2.5 wt% [94,95]. Such performance most often is for natural gas compositions, and little is known about how biogas will affect the sorption capacity for sulfur. Furthermore, water and CO_2 are strongly adsorbed on zeolites and, therefore, the gas to be treated needs to be free of moisture [24,96]. Data on adsorption of halogens on carbon only confirmed the results in our study that vinyl chloride and, in particular, low molecular weight halogens, such as chloromethane and chloroethane, are poorly adsorbed on many types of activated carbon [45,61,83,95].

In the system studied here, all sulfur and chlorinated species not captured by the carbon bed are removed by the high temperature polisher. Such a clean-up process has been used to treat biogas in several case studies for fuel cell systems [45,49,50]. Organic sulfur and chlorine are first reacted with hydrogen over a hydroprocessing catalyst (HDS) (such as Ni–Mo or Co–Mo supported on alumina) and converted to H_2S and HCl, respectively. These species are then removed by using sulfur and chlorine adsorbents (i.e.,

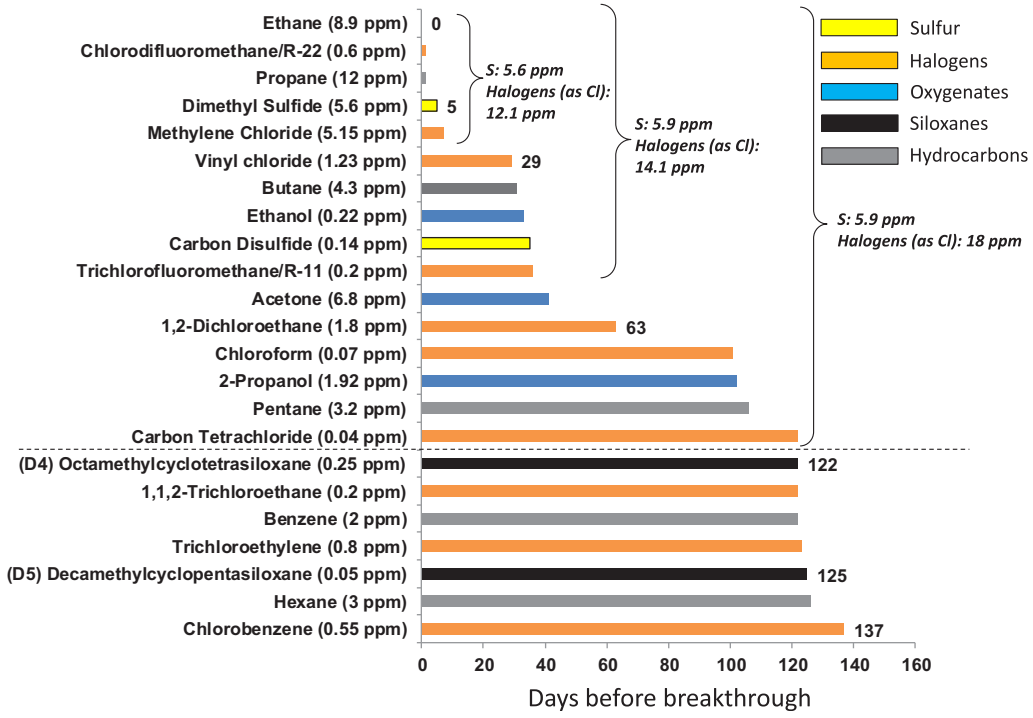

Fig. 14. Breakthrough time for weakly adsorbed species on activated carbon (average LFG composition).

ZnO-based sorbents for H_2S, and Al_2O_3 with metal oxides for chlorine). Screening tests reported in the literature with 500 ppm of H_2S and HCl over commercial adsorbents indicated a removal capacity of ~8–10 wt% for sulfur and chlorine, each, before breakthrough [97]. The tests were conducted at 270–350 °C and ambient pressure.

The effectiveness of the hydroprocessing catalyst depends on the partial pressure of hydrogen, temperature, and the concentrations of the trace impurities. He et al. [49] observed good activity for the hydroprocessing catalyst with tests using simulated landfill gas (~150 ppm halogens, and 25 ppm DMS and COS each) operating at 340 °C and using a hydrogen partial pressure of ~5 kPa. Oxygen in the gas (1%) and even moisture showed no noticeable effect on the activity of the catalysts and subsequent sorbents.

Some of the base case design parameters and assumptions for the high temperature polisher are as follows:

- Temperature: 330 °C
- H_2 partial pressure for HDS: 5 kPa
- Sulfur removal media: G-72E (5 wt% sulfur capacity before breakthrough)
- Chlorine removal media: G-92C (5 wt% chlorine capacity before breakthrough)
- Dual beds for adsorbents for continued operation during media replacement.

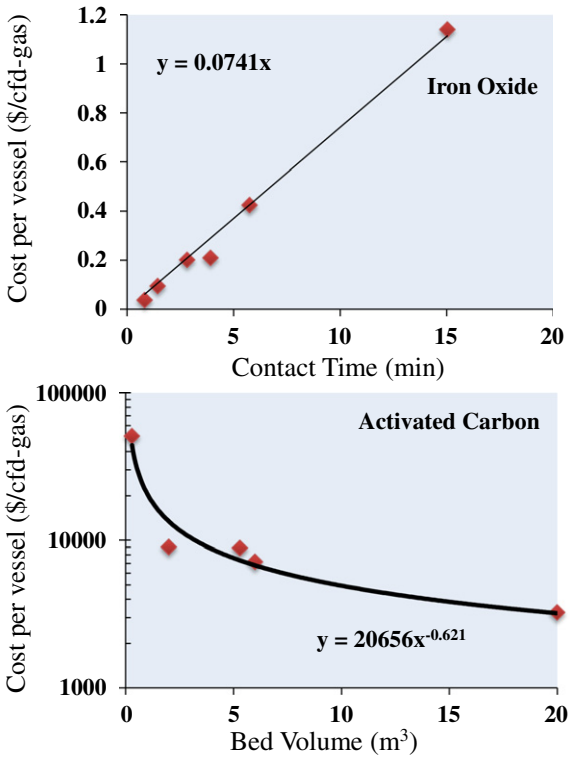

Fig. 15. Capital cost for iron oxide and carbon vessel as function of contact time. Symbols denote cost data from the literature.

5. Economic analysis

5.1. Cost factors and financial inputs

Along with the cost factors that impact the economics of the plant, the analysis evaluated the sensitivity of the cost of electricity to the impurity levels in the biogas. Cost factors included in the analysis were

(a) Capital costs for the clean-up process and fuel cell system (including stack replacement).
(b) Variable costs for maintenance and replacement of spent media.

Analytical costs (i.e., grab sampling of the biogas) as well as incentives or energy tax credits were not included in this analysis.

Cost data were obtained from the published literature [46,54,68,97–107]. The capital costs for the iron oxide and the activated carbon vessels are shown in Fig. 15. The cost includes piping and instrumentation and assumes that 2 vessels will be used in series (lead and lag). The capital cost for iron oxide beds increases linearly with vessel size, suggesting specialized beds and custom engineering for each project. In contrast, the capital cost for the carbon beds shows some economies of scale, possibly because of wide applications and sizes of such beds for VOC control. Chiller capital costs (excluding compressor/blowers) are $500–700 per scfm for flow rates above 35 scfm [100,106]. For small flow rates, the chillers can cost up to $3000 per scfm, as those units are overdesigned in relation to the flow capacity [46,106]. For the high temperature polisher, we have used the system costs estimated by Directed Technologies Inc. (currently Strategic Analysis, Inc) for natural gas polishing[3] [108]. The cost includes piping and vessels (2 in parallel), and also includes a heat exchanger and HDS catalyst.

[3] Costs were scaled based on the ratio of the flow rates (Qr): $\text{Cost} = \text{Cost}_0 \times (\text{Qr})^{0.6}$.

(a) The cost for carbon onsite replacement services is reported to be $4–5 per kg or virgin activated carbon, approximately twice the cost of the media ($2/kg) [68,99].
(b) The cost for the iron oxide media (SulfaTreat) is reported to be ~$1/kg [54,101,107]. Disposal costs are estimated to be 25–100% of the media cost [102].
(c) Sulfur removal media (G-72E) cost: $8.8/kg [97].
(d) Chlorine removal media (G-92C) cost: $2.2/kg [97].

Disposal costs for the high temperature polisher media were not reported. Considering that disposal/regeneration may cost as much as the media itself, we have assumed that all replacement costs equal the cost of the media. Tables 6 and 7 summarize the financial data and assumptions used for the economic analysis.

5.2. Cost of electricity – base case (ADG)

We used the H2A Fuel Cell Power (FCPower) model to calculate the cost of electricity for the base case ADG system described in this paper. The FCPower model is a financial tool for analyzing high temperature, fuel cell-based systems [109]. It is developed by the U.S. DOE (Department of Energy) and available free for use at DOE's website. Fig. 16 shows the cost of electricity as a function of the fuel cell system cost. The clean-up cost for the base case adds ~1.8 cents/kWh to the cost of electricity, representing ~20% of the total cost (10.5 cents/kWh). The fuel cell system cost for the base case was assumed to be $3800/kW; this is higher than the cost projected for 2010 by the FCpower tool ($2900/kW) but more in line with the current cost estimates for a DFC-300 unit operating on natural gas ($4500/kW) [105]. The cost for the DFC-300, however, also includes clean-up equipment for natural gas (sulfur removal) estimated at ~$400 kW. The cost of electricity in

Table 6
Financial inputs and cost factor for the fuel cell system.

Characteristics	Value	Units
Financial inputs		
Reference year	2005	Year
Start-up year	2010	Year
Plant life	20	Years
Depreciation schedule length	5	Years
Depreciation type	MACRS	–
Total tax rate	38.90	%
Installation cost[a]	20	%
Fuel cell system		
Plant design capacity	300	kW
Electrical efficiency[b]	46.3–47	%-fuel LHV
Total efficiency	70	%-fuel LHV
Fuel cell system capital cost (uninstalled)[c]	1,140,000	$
Heat value[d]	10	$/MMBtu

[a] Installation cost based on total direct depreciable capital cost (Fuel cell system + clean-up).
[b] (47% for ADG and 46.3% for LFG).
[c] Includes balance of plant components. Fuel cell system O&M: 1.5% of installed cost/year + 8% of installed cost every 2 years (see H2A FCPower Model [109]).
[d] Waste heat credit at 85% yearly utilization.

the analysis includes a heat credit of 1.4 cents/kWh (thermal). Here, we assume 85% yearly utilization [110] of the waste heat recovered from the process (colder climate) and valued at $10 MMBtu.

Table 7
Capital and maintenance costs for the clean-up system.

Characteristics	ADG	LFG	Unit
Fuel flow & methane content			
Flow rate (dry basis)	2570	3130	Nm^3/day
Methane content (%)	60	50	%-vol
Iron oxide			
H_2S Concentration	400	62	ppm
Vessel contact time	120	60	s
Adsorption capacity	0.0828	0.0715	g-S/g-media
Replacement frequency	27	72	weeks/bed
Annual adsorbent consumption	7030	1323	kg/year
Capital cost (2-vessel system)[a] (uninstalled)	27,500	13,730	$
Adsorbent cost[b]	2	2	$/kg
Total annual media cost[c]	7520	3080	$/year
Moisture removal			
Capital cost chiller/condenser[a] (uninstalled)	36,600	36,000	$
Activated carbon			
Adsorbent amount	700	700	kg/bed
Replacement frequency	165	122	weeks/bed
Annual adsorbent consumption	1548	2094	kg/year
Capital cost (2-vessel system)[a] (uninstalled)	48,800	48,800	$
Adsorbent cost[b]	4	4	$/kg
Total annual media cost[c]	7521	10,172	$/year
High temperature polisher			
Adsorbent amount (sulfur guard)	2.2	160	kg/bed
Adsorbent amount (chlorine guard)	13.3	500	kg/bed
Replacement frequency (for both guards)	1	1	year/bed
Capital cost (2-vessel system)[a,d] (uninstalled)	12,800	18,300	$
Adsorbent (sulfur guard) cost[b]	17.6	17.6	$/kg
Adsorbent (chlorine guard) cost[b]	4.4	4.4	$/kg
Total annual media cost[c]	150	5620	$/year

[a] Maintenance cost includes 2% of installed cost/year.
[b] Includes replacement/disposal costs (100% of media cost).
[c] Cost includes a handling fee of $600/replacement.
[d] Capital cost includes HDS catalyst.

Operating on natural gas instead of ADG (assuming no clean-up costs) and with a fuel cost of $10 MMBtu,[4] the corresponding cost of electricity increases to ~16.2 cents/kWh. Clearly, the costs for the clean-up in the case of ADG are more than offset by the zero cost of fuel, at least for the base case.

The pie chart in Fig. 16 shows the breakdown of the clean-up costs for the base case. Removal of H_2S and mercaptans (with iron oxide), which represents the bulk of the impurities in ADG, represents nearly half of the clean-up cost. The carbon beds add 34% to the cost of clean-up. The high temperature polisher adds but a small fraction to the clean-up cost (~5%). The average concentration of organic sulfur and halogens in ADG is low to begin with, and the combined concentration of organic sulfur and halogens not captured by the carbon bed is less than 1 ppm for the base case.

The sensitivity of the cost of electricity to some of the operating parameters and cost inputs is shown in Fig. 17. Fig. 17a shows the sensitivity for the iron oxide media (H_2S) removal. The media cost is important—a 50% increase in media costs leads to a 0.3 cents/kWh increase in the cost of electricity. Higher concentrations of H_2S can quickly escalate the operating costs due to the need for frequent media replacement.

The utilization of the media is also related to the bed sizes. Decreasing the volume of the bed (contact time of 60 s) decreases the capital cost for the vessels, however, the utilization of the adsorbent decreases rapidly when the contact time is lowered (the gas spends less time in the bed). Thus, the higher operating costs more than offset the savings in capital investment.

For H_2S concentration higher than those considered in this analysis, other sulfur removal technologies may be more suitable [24]. More capital intensive technologies may be better suited for larger plants than the base case investigated here (300 kWe). Another alternative may be to use other sulfur removal strategies preceding the iron oxide media beds, e.g., using iron salts to precipitate the bulk of the sulfur in the digester itself.

The sensitivity of the cost of electricity to the low temperature polisher (chiller/activated carbon) beds is shown in Fig. 17b. The replacement frequency for the carbon beds is directly related to the operating parameters (pressure, temperature, RH) and the trace contaminant concentrations in the biogas. In contrast to that for the iron oxide media, the capital cost for the low temperature polisher is higher, and it is more sensitive to variations in the operating parameters. This may be because custom-sized chillers may not be available leading to the use of overdesigned units in the plant. Also, the gas may need to be dried even further if the adsorption capacity of the media is particularly sensitive to moisture. The cost of further drying may reduce the operating costs for media replacement, but it will increase the capital investment and, therefore, the cost of electricity.

5.3. Cost of electricity – LFG

The cost of electricity from a 300 kW MCFC operating on landfill gas was evaluated using the average composition of LFG (Table 3). This was done to compare the associated clean-up costs with the ADG case. The clean-up system was kept unchanged but the bed sizes for the iron oxide media and for the high temperature polisher (sulfur and chlorine guards) were adjusted for the different impurity concentrations in LFG. The replacement interval also changed for some of the beds due to the change in the impurity matrix.

Table 7 compares the costs and replacement intervals for the ADG and LFG cases. For the iron oxide media, the bed size is smaller

[4] Fuel cost based on commercial natural gas (~$9.7 MMBtu as of AUG 2011). www.eia.gov.

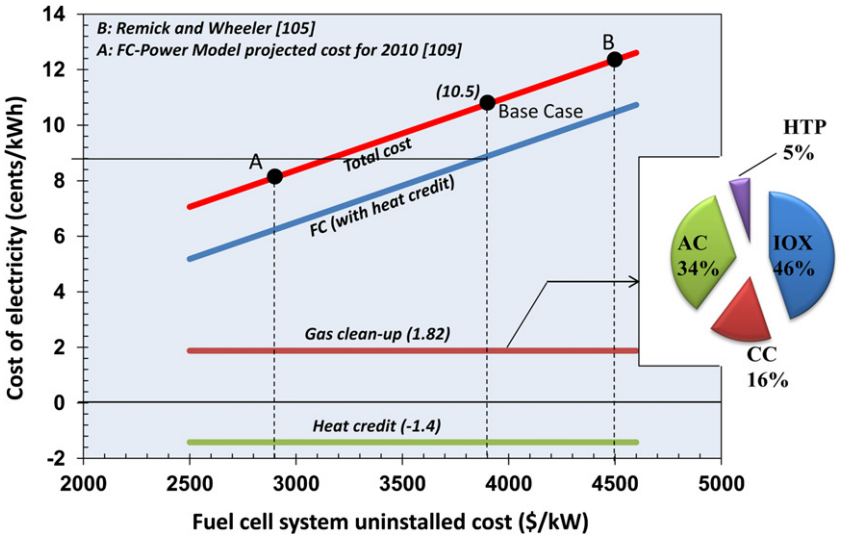

Fig. 16. Cost of electricity as function of fuel cell system capital cost. Power plant operates on ADG (average concentration). Pie chart denotes contributions to clean-up costs (%) AC = activated carbon, CC = chiller/condenser, IOX = iron oxide, HTP = high temperature polisher.

for the LFG, due to its lower concentration of H_2S (62 ppm). This decreases the utilization of the media but the capital cost is lower. The replacement interval increases to 72 weeks, compared to 26 weeks for the ADG case. The carbon media replacement frequency was based on D4 as the limiting species and the change-out occurred after 122 days. Because of the higher concentration of organic sulfur and halogens that enter the high temperature polisher, however, the size of the adsorbents increased substantially as compared to the ADG case.

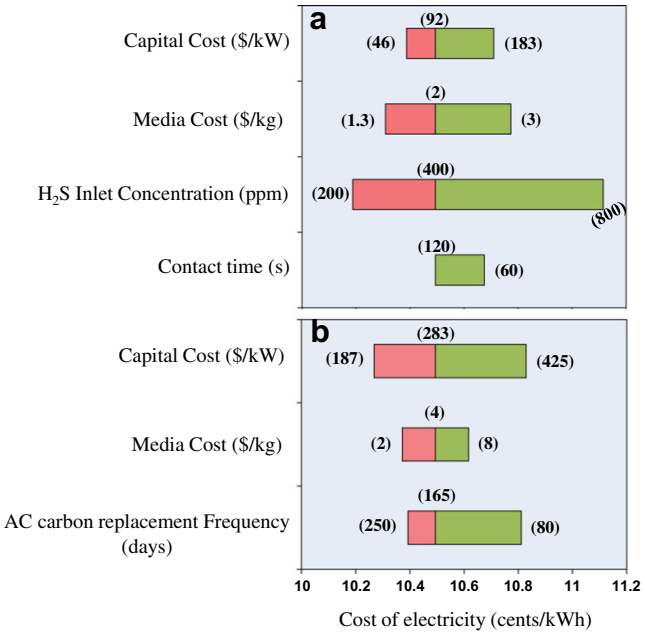

Fig. 17. Cost sensitivity of electricity for an MCFC operating on ADG. (a) Effect of cost and operating parameters on the primary clean-up step (H_2S removal in iron oxide beds). (b) Effect of cost and operating parameters on the low temperature polisher (capital cost includes chiller/condenser and carbon beds).

Fig. 18 shows the calculated cost of electricity for both the ADG and LFG cases (average concentrations of impurities). The cost of electricity from LFG and ADG is very similar (to within 0.2 cents/kWh). However, the distribution of the costs for the clean-up steps reflects the differences in their impurity levels. For ADG with its higher H_2S content, the cost for the H_2S clean-up step is ~4 times that in the LFG case. The savings in lower H_2S concentration for LFG, on the other hand, are offset by the higher cost of carbon media and, in particular, the cost of the high temperature polisher. The higher concentrations of organic sulfur and chlorine in LFG add ~0.3 cents/kWh to the cost of the polisher. The carbon media is marginally more expensive for LFG as the replacement frequency has increased. The activated carbon captures more chlorine than silica in LFG, while the opposite is observed for ADG.

It is expected that system optimizations will enable the further reduction of the cost of clean-up. Unfortunately, each of these plants has to be customized to meet the specific impurity content of the feed gas. The differences in bed sizes for ADG and LFG are a striking example. Furthermore, a particular clean-up strategy may not suit all fuel cell systems. A high temperature polisher may be more adaptable to low temperature fuel cells (i.e., PAFC) that reform the fuel to a H_2 rich gas outside the fuel cell stack, but may be more complicated for fuel cells that internally reform the fuel in the stack.

The service life of the iron oxide beds may be determined cost effectively by H_2S sensors or standardized analytical equipment (e.g., lead acetate tape, draeger tubes). Determining the service life of carbon may be more complicated, and it may require expensive analytical procedures.

While the trace contaminants in the fuel greatly affect the performance and degradation of the fuel cell system, variations in the main components of the gas, i.e., CH_4 and CO_2, impact the systems significantly since they determine the calorific value of the gas [24,111]. Such variations can cause irregular problems and lead to a shut-down of the fuel cell system. Solutions to this problem include storage of biogas to allow amounts of biogas with different heating values to equalize, or switching periodically to natural gas or propane when the calorific value starts to greatly deviate from normal values — all of which can add to the complexity and operating costs of the plant.

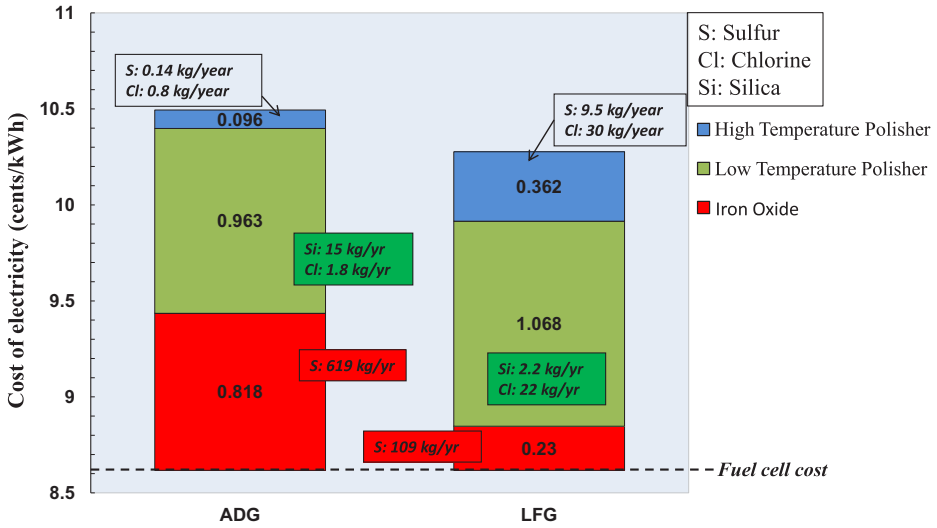

Fig. 18. Contributions to the cost of electricity for an MCFC operating on ADG and LFG (average concentrations of impurities for each source gas).

6. Summary and conclusions

This paper presents the results of a study to estimate the impact of impurities in biogas on the generation of electricity in stationary fuel cell systems. The study included a review of the literature data available on impurities found in biogas, especially in anaerobic digester gas and landfill gas. A detailed listing of this information, along with the effects of impurities on fuel cell performance and durability, can be accessed at: http://www.cse.anl.gov/FCs_on_biogas.

Impurities of particular concern are sulfur, siloxanes, and halides, because of their significant deleterious effects on the performance and durability of fuel cell systems. Moisture, higher hydrocarbons, aromatics, alcohols, etc., which are also present in the biogas, do not directly damage the fuel cell or diminish its performance; however, their presence reduces the capacity of the adsorbents that are typically used to capture the more deleterious species from the biogas.

The biogas clean-up strategies for fuel cell power generation systems have been reviewed. A generic process has been proposed, and this process has been used to conduct an economic analysis. This clean-up process begins with the removal of reduced sulfur, followed by moisture removal and adsorption beds to remove siloxanes and strongly adsorbed halocarbons on activated carbon. The remaining halocarbon and sulfur species not captured by the carbon beds are then removed by hydroprocessing at elevated temperatures, before the gas is fed into the fuel cell.

A base case process has been defined to conduct the economic analysis. The results show that the cost of electricity to be 10.5 and 10.3 cents/kWh from ADG and LFG, respectively, from a plant generating 300 kWe. The cost of gas clean-up represents ~20% of the cost of electricity. For the ADG case, the removal of H_2S (iron oxide bed) and siloxanes (carbon bed) contributes the most to that cost; whereas, for LFG, the siloxane removal (carbon bed) cost dominates.

Further technological development is necessary to help accelerate the deployment of biogas based fuel cell power generation developments.

- The activated carbon beds are replaced periodically, where the replacement interval is determined using a grab sample for the analysis of siloxanes. Development of continuous monitoring devices for these species would allow better use of the sorbent beds.
- Low temperature sorbents for the removal of halogen species are not effective for all species. Development of sorbents for these species that have high sorption capacities will preclude the need for a complex hydroprocessing strategy and would facilitate internal reforming.
- Data on adsorption properties of impurities on common sorbents are scarce in the published literature, especially for multicomponent systems. Such data are needed for greater accuracy in predicting impurity breakthrough and sorption capacity of these sorbents.

Acknowledgments

The authors would like to thank Fuel Cell Energy, Versa Power, and Acumentrics for their support and insight into some of the issues addressed in this project. This work was supported by the U.S. Department of Energy's Fuel Cell Technologies Program Office. Argonne National Laboratory is managed for the U.S. Department of Energy by UChicago Argonne, LLC, under contract DE-AC-02-06CH11357.

Appendix A. Supplementary material

Supplementary material associated with this article can be found, in the online version, at http://dx.doi.org/10.1016/j.energy.2012.06.031.

References

[1] Thorneloe S. Background information document for estimating emissions from municipal solid waste landfills – report EPA/600/R-08-116. Washington, DC: Eastern Research Group, Inc.. p. 108, www.nepis.epa.gov; 2008 [accessed 30.06.12].
[2] www.epa.gov/osw; 2009Municipal solid waste in the United States. Facts and Figures. p. 1–189. [accessed 15.05.12].
[3] www.epa.gov/outreach/lmop/; 2010Project development handbook: chapter 1 – landfill gas energy basics [accessed 15.05.12].
[4] Arnold M. Reduction and monitoring of biogas trace compounds. Vuorimiehentie: VTT Technical Research Centre of Finland; 2009. p. 84.
[5] Urban W, Lohmann H, Gomez JIS. Catalytically upgraded landfill gas as a cost-effective alternative for fuel cells. Journal of Power Sources 2009; 193(1):359–66.

[6] www.epa.gov/lmop. EPA-Landfill methane outreach program. [accessed 15.05.12].
[7] Appels L, Baeyens J, Degreve J, Dewil R. Principles and potential of the anaerobic digestion of waste-activated sludge. Progress in Energy and Combustion Science 2008;34(6):755–81.
[8] Stillwell AS, King CW, Webber ME, Duncan IJ, Hardberger A. The energy-water Nexus in Texas. Ecology Society 2011;16(1):945–62.
[9] Monteith HD, Bagley DM, MacLean HM, Kalogo Y. An assessment tool for managing cost-effective energy recovery from anaerobically digested wastewater solids. Alexandria, VA: The Water Environment Research Foundation. p. 235, www.werf.org; 2006 [accessed 30.06.12].
[10] www.epa.gov/chp/publications; 2011Opportunities for and benefits of combined heat and power at wastewater treatment facilities. Report prepared by: Eastern Research Group, Inc. (ERG) and Energy and Environmental Analysis, for the U.S. Environmental Protection Agency Combined Heat and Power Partnership; 2011. p. 48. [accessed 15.05.12].
[11] Pacific Gas and Electric Company. Energy baseline study for municipal wastewater treatment plants. San Francisco, CA: Report prepared by BASE Energy, Inc.. p. 43, www.pge.com; 2006 [accessed 30.06.12].
[12] Appleby AJ. Fuel cell technology: status and future prospects. Energy 1996; 21(7–8):521–653.
[13] Allen MR, Braithwaite A, Hills CC. Trace organic compounds in landfill gas at seven UK waste disposal sites. Environmental Science & Technology 1997; 31(4):1054–61.
[14] Parker T, Dottridge J, Kelly S. Investigation of the composition and emissions of trace components in landfill gas. Bristol, U.K.: Environment Agency, Rio House. p. 146, www.environment-agency.gov.uk; 2002 [accessed 30.06.12].
[15] Saber DL, Cruz KMH. Pipeline quality biomethane: North American guidance document for introduction of dairy waste derived biomethane into existing natural gas networks: Task 2. Des Plaines: Gas Technology Institute. p. 93, www.gastechnology.org; 2009 [accessed 30.06.12].
[16] Papadias DD, Ahmed S. Database of trace contaminants in LFG and ADG. Argonne National Laboratory. Excel files available for download at: http://www.cse.anl.gov/FCs_on_biogas; 2012 [accessed 15.05.12].
[17] www.lacsd.org/about/wastewater_facilities/jwpcp; 2001The LACSD experience with thermophilic digestion: start-up and operation of a full-scale reactor from mesophilic conditions [accessed 24.09.11].
[18] Osorio F, Torres JC. Biogas purification from anaerobic digestion in a wastewater treatment plant for biofuel production. Renewable Energy 2009; 34(10):2164–71.
[19] Peplin B, Walker G. Biocycle – renewable energy from organics recycling. In: 9th annual conference on renewable energy from organics recycling. Minneapolis, MN; 2009.
[20] Sasaki K, Adachi S, Haga K, Uchikawa M, Yamamoto J, Iyoshi A, et al. Fuel impurity tolerance of solid oxide fuel cells. ECS Transactions 2007;7(1): 1675–83.
[21] Brooke DN, Crookers MJ, Robertson S. Environmental risk assessment report: decamethylcyclopentasiloxane. Bristol, U.K.: Environment Agency, Rio House. p. 1–220, www.environment-agency.gov.uk; 2009 [accessed 30.06.12].
[22] McBean EA. Siloxanes in biogases from landfills and wastewater digesters. Canadian Journal of Civil Engineering 2008;35(4):431–6.
[23] Haga K, Adachi S, Shiratori Y, Itoh K, Sasaki K. Poisoning of SOFC anodes by various fuel impurities. Solid State Ionics 2008;179(27–32):1427–31.
[24] Lampe S. Assessment of fuel gas cleanup systems for waste gas fueled power generation. Palo Alto, CA: Electronic Power Research Institute. p. 108, www.epri.com; 2006 [accessed 30.06.12].
[25] Rasi S, Veijanen A, Rintala J. Trace compounds of biogas from different biogas production plants. Energy 2007;32(8):1375–80.
[26] Ciccoli R, Cigolotti V, Lo Presti R, Massi E, McPhail SJ, Monteleone G, et al. Molten carbonate fuel cells fed with biogas: combating H_2S. Waste Management 2010;30(6):1018–24.
[27] www.netl.doe.gov; 2004Fuel cell handbook. 7th ed. Morgantown, West Virginia: National Energy Technology Laboratory; 2004 [accessed 15.05.12].
[28] Haga K, Shiratori Y, Ito K, Sasaki K. Chlorine poisoning of SOFC Ni-cermet anodes. Journal of the Electrochemical Society 2008;155(12). B1233–B9.
[29] Watanabe T, Izaki Y, Mugikura Y, Morita H, Yoshikawa M, Kawase M, et al. Applicability of molten carbonate fuel cells to various fuels. Journal of Power Sources 2006;160(2):868–71.
[30] Abe J, Chaytors R, Clark C, Marshall C, Morgan E. Toward a renewable power supply: the use of bio-based fuels in stationary fuel cells. Washington, DC: Northeast Regional Biomass Program, www.nrbp.org; 2002 [accessed 30.06.12].
[31] Cayan FN, Zhi MJ, Pakalapati SR, Celik I, Wu NQ, Gemmen R. Effects of coal syngas impurities on anodes of solid oxide fuel cells. Journal of Power Sources 2008;185(2):595–602.
[32] Cigolotti V. Non-conventional waste-derived fuels for molten carbonate fuel cells: experimental investigations and technical-economical evaluations [Ph.D.]. Naples: University of Naples Federico II, www.fedoa.unina.it; 2009 [accessed 30.06.12].
[33] Desiduri. State of the air about the effects of impurities on MCFCs and pointing out of additional research for alternative fuel utilization. In: Proceedings of 1st international conference of fuel cell science, engineering and technology, April 21–23, 2003, Rochester NY; 2003.
[34] Krishnan G, Jayaweera P, Bao J, Perez J, Lau KH, Hornbostel M, et al. Effect of coal contaminants on solid oxide fuel system performance and service life. Morgantown, WV: SRI International/RTI International. p. 120, www.osti.gov; 2008 [accessed 30.06.12].
[35] Kubota K, Kuroda K, Akiyama K. Present status and future prospects of biogas powered fuel cell power units. Fuji Electric Review 1996;49:68–72.
[36] Moreno A, McPhail S, Bove R. International status of Molten Carbonate Fuel Cell (MCFC) technology. Rome: Italian National Agency for New Technologies. Energy and the Environment 2008:39.
[37] Spiegel RJ, Preston JL. Test results for fuel cell operation on anaerobic digester gas. Journal of Power Sources 2000;86(1–2):283–8.
[38] Srinivasan S, Dave BB, Murugesamoorthi KA, Parthasarathy A, Appleby AJ. Overview of fuel cell systems. In: Blomen LJMJ, Mugerwa MN, editors. Fuel cell systems. New York: Plenum Press; 1993. p. 42–7.
[39] Staffell I. Performance review of phosphoric acid fuel cells. Birmingham, England: University of Birmingham. p. 9, http://works.bepress.com/iain_staffell/2/; 2007 [accessed 30.06.12].
[40] Tomasi C, Baratieri M, Bosio B, Arato E, Baggio P. Process analysis of a molten carbonate fuel cell power plant fed with a biomass syngas. Journal of Power Sources 2006;157(2):765–74.
[41] Veyo SE. Evaluation of fuel impurity effects on solid oxide fuel cell performance. Pittsburgh, PA: Westinghouse. p. 59, www.osti.gov; 1998 [accessed 30.06.12].
[42] King County. King county fuel cell demonstration project. Final Report Prepared for the U.S. Environmental Protection Agency. Seattle, WA: King County Department of Natural Resources and Parks – Wastewater Treatment Division. p. 433, www.kingcounty.gov/environment/wastewater/ResourceRecovery/Energy/Innovations/FuelCell.aspx; 2009 [accessed 30.06.12].
[43] Spiegel RJ, Preston JL. Technical assessment of fuel cell operation on landfill gas at the Groton, CT, landfill. Energy 2003;28(5):397–409.
[44] Spiegel RJ, Thorneloe SA, Trocciola JC, Preston JL. Fuel cell operation on anaerobic digester gas: conceptual design and assessment. Waste Management 1999;19(6):389–99.
[45] Steinfeld G, Sanderson R. Landfill gas cleanup for carbonate fuel cell power generation. Golden, Colorado: National Renewable Energy Laboratory. NREL/SR-570-26037, www.nrel.gov/docs/legosti/fy98/26037.pdf; 1998 [accessed 30.06.12].
[46] www.oregon.gov/energy/renew; 2010Spring street sewage treatment plant. Klemath Falls: biogas energy management study – final submittal. p. 203. [accessed 28.09.11].
[47] Deed C, Gronow J, Rosevear A, Braithwaite P, Smith R, Stanley P. Guidance on gas treatment technologies for landfill gas engines. Bristol, U.K.: Environment Agency Rio House. p. 72, www.environment-agency.gov.uk; 2004 [accessed 30.06.12].
[48] Zappini G, Cocca P, Rossi D. Performance analysis of energy recovery in an Italian municipal solid waste landfill. Energy 2010;35(12):5063–9.
[49] He CT, Herman DJ, Minet RG, Tsotsis TT. A catalytic/sorption hybrid process for landfill gas cleanup. Industrial & Engineering Chemistry Research 1997; 36(10):4100–7.
[50] Spiegel RJ, Preston JL. Technical assessment of fuel cell operation on anaerobic digester gas at the Yonkers, NY, wastewater treatment plant. Waste Management 2003;23(8):709–17.
[51] Spiegel RJ, Preston JL, Trocciola JC. Fuel cell operation on landfill gas at Penrose power station. Energy 1999;24(8):723–42.
[52] Lukas MD, Lee KY, Ghezel-Ayagh H. An explicit dynamic model for direct reforming carbonate fuel cell stack. IEEE Transactions on Energy Conversion 2001;16(3):289–95.
[53] Lukas MD, Lee KY, Ghezel-Ayagh H. Modeling and cycling control of carbonate fuel cell power plants. Control Engineering Practice 2002;10(2): 197–206.
[54] Abatzoglou N, Boivin S. A review of biogas purification processes. Biofuels Bioproducts & Biorefining 2009;3(1):42–71.
[55] Choi DK, Choi DY, Lee JW, Jang SC, Ahn BS. Adsorption dynamics of hydrogen sulfide in impregnated activated carbon bed. Adsorption-Journal of the International Adsorption Society 2008;14(4–5):533–8.
[56] Cruz AJ, Pires J, Carvalho AP, De Carvalho MB. Physical adsorption of H_2S related to the conservation of works of art: the role of the pore structure at low relative pressure. Adsorption-Journal of the International Adsorption Society 2005;11(5–6):569–76.
[57] Yan R, Chin T, Ng YL, Duan H, Liang DT, Tay JH. Influence of surface properties on the mechanism of H_2S removal by alkaline activated carbons. Environmental Science & Technology 2004;38(1):316–23.
[58] Truong LVA, Abatzoglou N. A H_2S reactive adsorption process for the purification of biogas prior to its use as a bioenergy vector. Biomass and Bioenergy 2005;29(2):142–51.
[59] Carberry JJ, Varma A. Chemical reaction and reactor engineering. New York: Mercel Dekker; 1987. p. 293–365.
[60] Levenspiel O. Chemical reaction engineering. New York: John Wiley & Sons; 1972.
[61] Shin HC, Park JW, Park K, Song HC. Removal characteristics of trace compounds of landfill gas by activated carbon adsorption. Environmental Pollution 2002;119(2):227–36.
[62] Rudisill EN, Hacskaylo JJ, Levan MD. Coadsorption of hydrocarbons and water on BPL activated carbon. Industrial & Engineering Chemistry Research 1992; 31(4):1122–30.
[63] Qi N, Levan MD. Coadsorption of organic compounds and water vapor on BPL activated carbon. 5. Methyl ethyl ketone, methyl isobutyl ketone, toluene,

and modeling. Industrial & Engineering Chemistry Research 2005;44:3733–41.
[64] Lodewyckx P, Vansant EF. Influence of humidity on adsorption capacity from the Wheeler–Jonas model for prediction of breakthrough times of water immiscible organic vapors on activated carbon beds. American Industrial Hygiene Association Journal 1999;60(5):612–7.
[65] Cal MP, Rood MJ, Larson SM. Gas phase adsorption of volatile organic compounds and water vapor on activated carbon cloth. Energy & Fuels 1997;11(2):311–5.
[66] Schweigkofler M, Niessner R. Removal of siloxanes in biogases. Journal of Hazardous Materials 2001;83(3):183–96.
[67] Ajhar M, Travesset M, Yuce S, Melin T. Siloxane removal from landfill and digester gas – a technology overview. Bioresource Technology 2010;101(9):2913–23.
[68] United States Environmental Protection Agency. EPA air pollution control cost manual. North Carolina: Office of Air Quality Planning and Standards. EPA/452/B-02-001. p. 752, www.epa.gov/ttncatc1/dir1/c_allchs.pdf; 2002 [accessed 30.06.12].
[69] Wood GO. Activated carbon adsorption capacities for vapors. Carbon 1992;30(4):593–9.
[70] Ye XH, Qi N, Ding YQ, LeVan MD. Prediction of adsorption equilibrium using a modified D–R equation: pure organic compounds on BPL carbon. Carbon 2003;41(4):681–6.
[71] Matsui T, Imamura S. Removal of siloxane from digestion gas of sewage sludge. Bioresource Technology 2010;101:S29–32.
[72] Tower P. Removal of siloxanes from landfill gas by SAG™ polymorphous porous graphite treatment systems. In: SWANA 26th landfill gas symposium; 2003. p. 10.
[73] Wood GO. Review and comparisons of D/R models of equilibrium adsorption of binary mixtures of organic vapors on activated carbons. Carbon 2002;40(3):231–9.
[74] Poling BE, Prausnitz JM, O'Connell JP. The properties of gases and liquids. 5th ed. NewYork: McGraw Hill; 2001.
[75] Wood GO. Affinity coefficients of the Polanyi/Dubinin adsorption isotherm equations – a review with compilations and correlations. Carbon 2001;39(3):343–56.
[76] Bell JG, Zhao XB, Uygur Y, Thomas KM. Adsorption of chloroaromatic models for dioxins on porous carbons: the influence of adsorbate structure and surface functional groups on surface interactions and adsorption kinetics. The Journal of Physical Chemistry C 2011;115(6):2776–89.
[77] Boulinguiez B, Le Cloirec P. Adsorption on activated carbons of five selected volatile organic compounds present in biogas: comparison of granular and fiber cloth materials. Energy & Fuels 2010;24:4756–65.
[78] Chiou CT, Reucroft PJ. Adsorption of phosgene and chloroform by activated and impregnated carbons. Carbon 1977;15(2):49–53.
[79] Grant RJ, Manes M, Smith SB. Adsorption of normal paraffins and sulfur compounds on activated carbon. AIChE Journal 1962;8:403–6.
[80] Himeno S, Urano K. Determination and correlation of binary gas adsorption equilibria of VOCs. Journal of Environmental Engineering 2006;132(3):301–8.
[81] Lavanchy A, Stoeckli F. Dynamic adsorption of vapour mixtures in active carbon beds described by the Myers–Prausnitz and Dubinin theories. Carbon 1997;35(10–11):1573–9.
[82] Lu X, Jaroniec M, Madey R. Use of adsorption-isotherms of light normal alkanes for characterizing microporous activated carbons. Langmuir 1991;7(1):173–7.
[83] Mahle JJ, Buettner LC, Friday DK. Measurement and correlation of the adsorption equilibria of refrigerant vapors on activated carbon. Industrial & Engineering Chemistry Research 1994;33(2):346–54.
[84] Noll KE, Wang D, Shen T. Comparison of 3 methods to predict adsorption-isotherms for organic vapors from similar polarity and nonsimilar polarity reference vapors. Carbon 1989;27(2):239–45.
[85] Scamehorn JF. Removal of vinyl-chloride from gaseous streams by adsorption on activated carbon. Industrial & Engineering Chemistry Process Design and Development 1979;18(2):210–7.
[86] Schindler BJ, Buettner LC, LeVan MD. Transition to Henry's law in ultra-low concentration adsorption equilibrium for n-pentane on BPL activated carbon. Carbon 2008;46(10):1285–93.
[87] Seaton NA, He YF, Yun JH. Adsorption equilibrium of binary methane/ethane mixtures in BPL activated carbon: isotherms and calorimetric heats of adsorption. Langmuir 2004;20(16):6668–78.
[88] Stoeckli F, Wintgens D, Lavanchy A, Stockli M. Binary adsorption of vapours in active carbons described by the combined theories of Myers–Prausnitz and Dubinin (II). Adsorption Science & Technology 1997;15(9):677–83.
[89] Taqvi SM, Appel WS, LeVan MD. Coadsorption of organic compounds and water vapor on BPL activated carbon. 4. Methanol, ethanol, propanol, butanol, and modeling. Industrial & Engineering Chemistry Research 1999;38(1):240–50.
[90] Urano K, Omori S, Yamamoto E. Prediction method for adsorption capacities of commercial activated carbons in removal of organic vapors. Environmental Science & Technology 1982;16(1):10–4.
[91] Ortega DR, Subrenat A. Siloxane treatment by adsorption into porous materials. Environmental Technology 2009;30(10):1073–83.
[92] Wood GO, Snyder JL. Estimating service lives of organic vapor cartridges III: multiple vapors at all humidities. Journal of Occupational and Environmental Hygiene 2007;4:363–74.
[93] Papadias DD, Ahmed S, Kumar R, Joseck F. Hydrogen quality for fuel cell vehicles – a modeling study of the sensitivity of impurity content in hydrogen to the process variables in the SMR–PSA pathway. International Journal of Hydrogen Energy 2009;34:6021–35.
[94] Alptekin G, Jayaraman A, Dubovik M, Schaefer M, Ware M, Amalfitano R. Sorbents for natural gas desulfurization. ECS Transactions 2008;12(1):563–70.
[95] Hernandez SP, Scarpa F, Fino D, Conti R. Biogas purification for MCFC application. International Journal of Hydrogen Energy 2011;36(13):8112–8.
[96] Montanari T, Finocchio E, Salvatore E, Garuti G, Giordano A, Pistarino C, et al. CO2 separation and landfill biogas upgrading: a comparison of 4A and 13X zeolite adsorbents. Energy 2011;36(1):314–9.
[97] Newby RA, Lippert TE, Slimane RB, Akpolat OM, Pandya K, Lau FS, et al. Novel gas cleaning/conditioning for integrated gasification combined cycle. Report prepared by Siemens Westinghouse Power Corporation & Gas Technology Insitiute for the U.S. Department of Energy – National Energy Technology Laboratory. DOE Award Number: DE-AC26-99FT40674. p. 203, www.netl.doe.gov/technologies/coalpower/gasification/projects/gas-clean/docs/BaseProgramFinalReport.PDF; 2001 [accessed 30.06.12].
[98] Bluestem Solid Waste Agency. Anaerobic digestion feasability study. Bluestem Solid Waste Agency and Iowa Department of Natural Resources. p. 249, www.scribd.com/doc/51290973/bluestem; 2004 [accessed 30.06.12].
[99] Carbtrol Corporation. Activated carbon adsorption for treatment of VOC Emissions. In: 13th Annual EnviroExpo. Boston, MA; 2001. p. 4.
[100] CH2MHILL & Itron. Process selection report for wastewater treatment plants. Santa Ana, CA: Prepared for California Energy Comission. Contract No. 500-00-036. p. 57, www.pierminigrid.org/FinalDeliverables/Project22/Task2.2.1/Task2.2.1_ProcessSelection_FinalReport.pdf; 2003 [accessed 30.06.12].
[101] GC Environmental. Available control technologies for H_2S removal from landfill gas. Protland, OR: Prepared for Recology, GCE. Project No. 1332. p. 10, yosemite.epa.gov; 2010 [accessed 30.06.12].
[102] Kellog MW. GRI scavenger CalcBase™ software. Chicago, Illinois: Gas Research Institute; 1996. GRI Project #96/0482.
[103] Malcom Pirnie. Feasibility study of a pilot testing program for emission control biogas cleaning at a NYCDEP water pollution control plant. Albany, NY: Report prepared for: The New York State Energy Research and Development Authority (NYSERDA 9402). p. 47, www.nyserda.ny.gov/Publications.aspx; 2008 [accessed 30.06.12].
[104] Meyers RA. Encyclopedia of environmental analysis and remediation;, ISBN 978-0-471-11708-7; 1998.
[105] Remick R, Wheeler D. Molten carbonate and phosphoric acid stationary fuel cells: overview and gap analysis. Golden, Colorado: National Renewable Energy Laboratory. NREL/TP-560-49072. p. 51, www.osti.gov/greenenergy; 2010 [accessed 30.06.12].
[106] Roloson BD, Scott NR, Bothi K, Saikkonen K, Zicari S. Biogas processing. Albany, New York: The New York State Energy Research and Development Authority (NYSERDA 7250). p. 93, www.nyserda.ny.gov/Publications.aspx; 2006 [accessed 30.06.12].
[107] Zicari S. Removal of hydrogen sulfide from biogas using cow-manure compost [Master of Science Thesis]. N.Y.: Cornell University; 2003 www.cornell.edu [accessed 30.06.12].
[108] Myers DB, Ariff GD, James BD, Lettow JS, Thomas CE, Kuhn RC. Cost and performance comparison of stationary hydrogen fueling appliances. Washington, D.C.: Prepared by Directed Technologies for the U.S. Department of Energy (Grant no. DE-FG01-99EE35099). p. 129, www.eere.energy.gov/hydrogenandfuelcells/pdfs/32405b2.pdf; 2002 [accessed 30.06.12].
[109] Steward D. Fuel cell power model for CHHP system economics and performance analysis (Presentation). Golden, CO: National Renewable Energy Laboratory (NREL). p. 21, www.eere.energy.gov/hydrogenandfuelcells/pdfs/renewable_hydrogen_workshop_nov16_steward.pdf; 2009 [accessed 30.06.12].
[110] Malcom Pirnie. Municipal wastewater treatment plant energy evaluation for ithaca area wastewater treatment facility. Buffalo, NY: Report prepared for The New York State Energy Research and Development Authority (NYSREDA Project No. 7185). p. 84, www.nyserda.ny.gov/Publications.aspx; 2005 [accessed 30.06.12].
[111] Nicolin F, Verda V. Lifetime optimization of a molten carbonate fuel cell power system coupled with hydrogen production. Energy 2011;36(4):2235–41.